JOURNAL OF GEOPHYSICAL RESEARCH, VOL. 114, D10201, doi:10.1029/2008JD010325, 2009

Meteorological processes forcing Saharan dust emission inferred from MSG-SEVIRI observations of subdaily dust source activation and numerical models

K. Schepanski,[1,2] I. Tegen,[1] M. C. Todd,[3] B. Heinold,[1] G. Bönisch,[4] B. Laurent,[1] and A. Macke[2]

Received 25 April 2008; revised 23 February 2009; accepted 4 March 2009; published 20 May 2009.

[1] Fifteen-minute Meteosat Second Generation (MSG) Spinning Enhanced Visible and Infrared Imager (SEVIRI) infrared dust index images are used to identify dust source areas. The observations of dust source activation (DSA) are compiled in a $1^\circ \times 1^\circ$ map for the Sahara and Sahel, including temporal information at 3-hourly resolution. Here we use this data set to identify the most active dust source areas and the time of day when dust source activation occurs most frequently. In the Sahara desert 65% of DSA (March 2006 to February 2008) occurs during 0600–0900 UTC, pointing toward an important role of the breakdown of the nocturnal low-level jet (LLJ) for dust mobilization. Other meteorological mechanisms may lead to dust mobilization including density currents initiated by deep convective systems which mobilize dust fronts (haboobs) occurring preferentially in the afternoon hours and cyclonic activities. The role of the nocturnal LLJ for dust mobilization in the Sahara is corroborated by regional model studies and analysis of meteorological station data.

Citation: Schepanski, K., I. Tegen, M. C. Todd, B. Heinold, G. Bönisch, B. Laurent, and A. Macke (2009), Meteorological processes forcing Saharan dust emission inferred from MSG-SEVIRI observations of subdaily dust source activation and numerical models, *J. Geophys. Res.*, *114*, D10201, doi:10.1029/2008JD010325.

1. Introduction

[2] Airborne mineral dust particles impact on several atmospheric processes mainly related to radiation and cloud microphysics [*Intergovernmental Panel on Climate Change*, 2007]. Thus, the atmospheric radiation budget is influenced by airborne dust particles directly and indirectly [e.g., *Tegen and Lacis*, 1996; *Sokolik and Toon*, 1996; *Miller and Tegen*, 1999]. Besides impacts on physical processes controlled mainly by optical and physical characteristics, deposited mineral dust can act as nutrient to marine and terrestrial ecosystems depending on to its mineralogical composition [*Claquin et al.*, 1999]. As a source of iron, mineral dust provides nutrients for oceanic microorganisms and influences terrestrial ecosystems [*Mahowald et al.*, 2005]. Ultimately, dust influences the global CO_2 cycle [e.g., *Fung et al.*, 2000; *Jickells et al.*, 2005].

[3] Consequently, an adequate description of source areas and meteorological processes controlling dust emission is a prerequisite for accurate estimation of dust aerosol effects, as well as for the understanding of the response of dust emission to changing climate conditions. The Sahara is the World's most important dust source area [e.g., *Prospero et al.*, 2002; *Washington et al.*, 2003; *Goudie and Middleton*, 2001; *Middleton and Goudie*, 2001] providing an estimated dust production of 40–70% of the global annual total [*Engelstaedter et al.*, 2006]. Physical, optical and mineralogical properties that are important for the climate impacts of dust are controlled by local geomorphology of dust source regions. As in situ measurement at all of the important dust source locations is impractical, remote sensing must be used to provide a comprehensive data set on Saharan dust sources.

[4] Since remote sensing offers retrievals of airborne dust, several approaches for dust source determination have been developed. Most commonly, data from low Earth orbiting satellites are used. Earlier attempts to derive the major dust source areas in the Sahara included the use of daily data sets of the absorbing Aerosol Index (AI) from ultraviolet (UV) radiance measurements of the Total Ozone Mapping Spectrometer (TOMS) [*Herman et al.*, 1997], and since September 2004 from the Ozone Monitoring Instrument (OMI) [*Torres et al.*, 2007]. As the index indicates airborne dust over the ocean as well as over land surfaces like desert areas, the AI has been used to determine dust source areas, characterized by high AI values [e.g., *Prospero et al.*, 2002; *Washington et al.*, 2003]. The main areas of high AI are located over topographic depressions, which have been parameterized as preferential dust sources for

[1] Leibniz Institute for Tropospheric Research, Leipzig, Germany.
[2] Leibniz Institute of Marine Sciences at University of Kiel (IFM-GEOMAR), Kiel, Germany.
[3] Department of Geography, University College London, London, UK.
[4] Max-Planck-Institute for Biogeochemistry, Jena, Germany.

0148-0227/09/2008JD010325$09.00

modeling applications [*Ginoux et al.*, 2001; *Tegen et al.*, 2002; *Zender and Newman*, 2003].

[5] In addition, satellite sensors measuring at visible wavelengths are also used. Notably, Moderate Resolution Imaging Spectroradiometer (MODIS) and Sea-viewing Wide Field-of-view Sensor (SeaWiFS) measurements are used to derive aerosol properties over bright-reflecting surfaces like deserts from the deep blue part of the shortwave spectrum using the ''Deep Blue'' algorithm [*Hsu et al.*, 2004]. Also, a daily noon-time Infrared (IR) Difference Dust Index (IDDI) calculated from Meteosat measurements has been used to derive dust source areas [*Brooks and Legrand*, 2000].

[6] Such results are useful, but the temporal resolution is limited to, at best, instantaneous observations at a fixed daytime slot. Dust mobilization is known to be forced by synoptic-scale, mesoscale and local-scale winds as well as near surface turbulent processes, which are highly variable in time and can usually not be resolved adequately from a single day sample. Therefore biases in estimates of mean aerosol properties may occur, especially near source regions. Here, we use estimates of dust source activation (DSA) derived from IR measurements from the Meteosat Second Generation (MSG) Spinning Enhanced Visible and Infrared Imager (SEVIRI) instrument with 15 min resolution to obtain dust source information for the Sahara [*Schepanski et al.*, 2007]. These data provide (1) identification of areas that are of major importance for dust mobilization and (2) information of the time of day when the mobilization occurs. This new data set reduces biases associated with poor temporal sampling characteristic of polar orbiting satellites. The space-time distribution of DSA enables inferences on possible meteorological processes responsible for dust emission to be drawn. This paper aims to determine the diurnal cycle of dust emission in the Sahara inferred from satellite observations and to relate this to associated meteorological controls. It is structured as following: Section 2 will give a short overview on dominant meteorological features, which are related to dust source activation, most notably the breakdown of the nocturnal low-level jet (LLJ). In section 3 we then describe the space/time distributions of observed dust source activations derived from the MSG dust product and relate this to the associated meteorological dynamics, notably the LLJ. The space-time occurrence of LLJs in wind observations from synoptic weather stations, and fields of regional- and global-scale atmospheric models is analyzed in section 4.

2. Meteorological Processes Leading to Dust Source Activation

[7] For Saharan dust mobilization, atmospheric processes on synoptic, regional, local as well as turbulent scales can force emission and atmospheric mixing of dust particles. All atmospheric processes forcing dust mobilization must generate wind speeds exceeding the local threshold velocity depending on surface roughness length, soil structure and vegetation [*Marticorena and Bergametti*, 1995]. In this section, important meteorological situations able to provide atmospheric conditions suitable for dust mobilization are described. These include the turbulent mixing of momentum from nocturnal low-level jets (LLJ), the Mediterranean cyclone [*Alpert and Ziv*, 1989], and convective activity [*Flamant et al.*, 2007].

2.1. Nocturnal Low-Level Jet

[8] LLJs are characterized by a horizontal wind speed maximum in the lowest few kilometers of the atmosphere [e.g., *Blackadar*, 1957; *Holton*, 1967; *Banta et al.*, 2006]. They are most commonly observed at nighttime and can occur over all continents above flat and complex terrain and may extend over tens to hundreds of kilometers [*Davis*, 2000; *May*, 1995]. Over the Sahara, LLJs occur under clear skies and low surface wind speed conditions [e.g., *Thorpe and Guymer*, 1977] and have been observed within the northeasterly ''Harmattan'' flow [*Washington and Todd*, 2005] and the southwesterly monsoon flow [*Parker et al.*, 2005]. LLJs can be caused by baroclinity associated with sloping terrain, splitting, ducting and confluence around mountain barriers, mountain and valley wind, and inertial oscillation [*Kraus et al.*, 1985]. The inertial oscillation is commonly observed between subgeostrophic conditions during daytime due to convective mixing and supergeostrophic conditions during nighttime caused by a frictional decoupling from the surface [e.g., *Banta et al.*, 2002, 2003; *Nappo*, 1991; *Mahrt*, 1999; *Blackadar*, 1957]. During calm nights with low surface wind speeds, near-surface air layers are well stratified and turbulence is suppressed. In such conditions, air layers above near-surface can be frictionally decoupled such that wind speed within this decoupled air layer is not influenced by surface friction [e.g., *Hoxit*, 1975; *Garratt*, 1992; *Mauritsen and Svensson*, 2007; *Mahrt*, 1999].

[9] After sunrise, convective turbulence arises with the onset of solar heating. The decoupled air layer aloft becomes frictionally coupled to the surface, and LLJ momentum is mixed down [*Blackadar*, 1957; *Lenschow and Stankov*, 1979]. High surface wind speeds occur as a consequence until the LLJ is degraded. This process causes a characteristic phase lag between the diurnal cycle of LLJ wind speeds and those at the surface. The LLJ peaks at nighttime while surface wind peaks in midmorning when LLJ momentum is mixed down to the surface [*Parker et al.*, 2005; *Washington et al.*, 2006; *Todd et al.*, 2008]. These surface winds can enhance dust mobilization if they exceed the threshold velocity and occur at a potential dust source area [e.g., *Westphal et al.*, 1988]. The importance of the LLJ in the Bodélé region for dust emission has been established by *Washington et al.* [2006]. However, nocturnal LLJ features are common in other locations across North Africa [*Parker et al.*, 2005] including the summertime southwesterly monsoon flow and are likely to play an important role for dust emission [*Bou Karam et al.*, 2008]. In many cases dust emission is associated with enhanced LLJs under specific synoptic conditions of anticyclonic ridging [e.g., *Washington and Todd*, 2005; *Milton et al.*, 2008].

2.2. Mediterranean Cyclone

[10] Especially in spring season, the temperature contrast between the North African coast and the Mediterranean Sea enhances a boundary layer (BL) baroclinity [*Pedgley*, 1972; *Alpert and Ziv*, 1989; *Trigo et al.*, 2002]. Cyclones are observed in connection with this temperature induced BL baroclinity, most frequently in spring when temperature

gradients are strongest. These typical spring cyclones are known as Sharav cyclone, Saharan depression or Khamsin depression. At least three mechanisms dominate the generation of such cyclones [e.g., *Thorncroft and Flocas*, 1997; *Alpert and Ziv*, 1989; *Prezerakos et al.*, 1990; *Dayan et al.*, 1991; *Pedgley*, 1972]: Large-scale interior baroclinity, BL baroclinity, and jet stream related circulations. The cyclone, characterized by an active warm front, is frequently associated with extremely high surface temperatures, heavy dust storms and low visibilities, and a shallow cold front, that is well defined at the surface by changes in temperature of 10–20 K. It moves quickly eastward (typically faster than 10 m s^{-1}) mostly following the North African coast [*Alpert et al.*, 1990; *Alpert and Ziv*, 1989]. Observations indicate a frequent occurrence of the cyclone on the leeward side east and south of the Atlas Mountains [*Barkan et al.*, 2005; *Prezerakos et al.*, 1990; *Alpert et al.*, 1990; *Alpert and Ziv*, 1989]. Hence, both lee effect of the mountains and coastal thermal gradient effect can explain the spring cyclogenesis, initiated by the presence of an upper level trough to the west [e.g., *Horvath et al.*, 2006; *Egger et al.*, 1995]. Dust source activations related to the dynamics of the lee cyclone can generally be initiated during the whole day, but the surface heating will strengthen moist convection during daytime [e.g., *Trigo et al.*, 2002].

2.3. Convective Activity

[11] During northern hemispheric summer, a heat low commonly develops over North Africa with a mean position centered near 20°N, 0°E. The Intertropical Convergence Zone (ITCZ) in terms of maximum rainfall area extends to about 15°N [e.g., *Nicholson*, 2000]. Large-scale sinking of air associated with the Hadley circulation is weak and the BL deep. Because of solar heating and moist air transported from the Gulf of Guinea northward by the southwest monsoon flow, deep moist convection develops with maximum activity in the afternoon [*Peters and Tetzlaff*, 1988]. Downbursts of cold, humid air related to deep moist convection can occur causing high surface wind speeds. Such density currents can propagate many hundreds of kilometers from the convective system and cause dust emission referred to as "haboob" events [*Sutton*, 1925; *Idso et al.*, 1972; *Droegemeier and Wilhelmso*, 1987; *Flamant et al.*, 2007; *Bou Karam et al.*, 2008]. As the occurrence of haboobs is related to the dynamics of moist convection, they are frequently observed during afternoons and evenings.

[12] Deep moist convection also occurs in mountain areas, notably near by the Atlas Mountains, because of orographic effects and blocking situations. Large-scale density currents have been observed with evaporative cooling of cloud particles or precipitation. This can lead to high surface wind speeds and dust emission [*Droegemeier and Wilhelmso*, 1987; *Knippertz and Martin*, 2005; *Knippertz et al.*, 2007, 2009]. During daytime, air can be cooled by evaporation. Cloud droplets blown out by high winds in cloud top levels evaporate in dry surroundings. Consequently temperature decreases: A dense air mass is generated and sinks down as far as the surrounding air density is lower. In case of mountain ridges located orthogonally to a strong general flow, convective clouds are formed on top of the mountain ridges and the foehn effect provides a dry and warm air mass on the leeward side of mountain ridge. These conditions lead to a high density difference between air cooled by evaporation and the surrounding air. The dense, cooled air mass sinks down and can be identified as strong gusts at surface levels. These gusts propagate about the foothills and cause dust mobilization [*Knippertz et al.*, 2007; *Knippertz et al.*, 2009; *Smith and Reeder*, 1988; *Charba*, 1974].

[13] Density currents provided by blown out clouds are limited to the mountain regions and occur most frequently during the afternoon when moist convection reaches maximum [*Knippertz et al.*, 2007]. Over the Sahara, they can be observed most frequently in the Atlas Mountains because of transport of moist air toward the mountains within the generally westerly circulation.

[14] Besides moist convection, dry convection occurring related to the Saharan heat low where low atmospheric moisture content inhibit cloud development is identified to account for dust source activation [*Engelstaedter and Washington*, 2007].

3. Spatiotemporal Dust Source Characteristics Inferred From Satellite Observations

[15] Measurements provided by geostationary satellites are suitable to locate and characterize dust source activity because of their regional coverage and high temporal resolution. High frequencies of temporal varying dust source activities point toward recurring meteorological features able to provide suitable conditions for dust mobilization.

3.1. Dust Source Activation From MSG-SEVIRI

[16] For dust source area detection we use the SEVIRI instrument on board the geostationary MSG Satellite, located at 3.5°W above the equator (see *Schmetz et al.* [2002] for a detailed description). The instrument provides narrowband visible and IR measurements at a sampling interval of 15 min with a spatial resolution of 3 km × 3 km at nadir. This high spatiotemporal resolution motivates the use of a MSG IR dust index, calculated from SEVIRI IR channels centered at 8.7 μm, 10.8 μm and 12.0 μm, to obtain information on dust source locations and activation over the Saharan desert between 5°N–40°N; 20°W–45°E (for a detailed description see *Schepanski et al.* [2007]). The dust index may be biased by variations in brightness temperature differences for dust at different heights. Here only qualitative information on presence or absence of dust is used. Individual dust plumes were identified from the SEVIRI dust product and tracked back to their initial location. The location of the dust source is determined by tracking back the dust plume indicated by the dust index to its point of first occurrence. The time of the first observations is taken as the time of dust source activation. From this information a frequency count was derived for each location. The DSA frequencies (fraction of DSA per day) were binned in a 1° × 1° gridded map at 3-h intervals [*Schepanski et al.*, 2007]. Each grid cell can only be counted as dust source once per day. This leads to a weighting of the observed time-of-day distribution toward the earlier activation. However, observations show that days when a grid cell denoted as active dust source can be counted as active more than once a day are seldom. On those days, an additional dust source activation independent

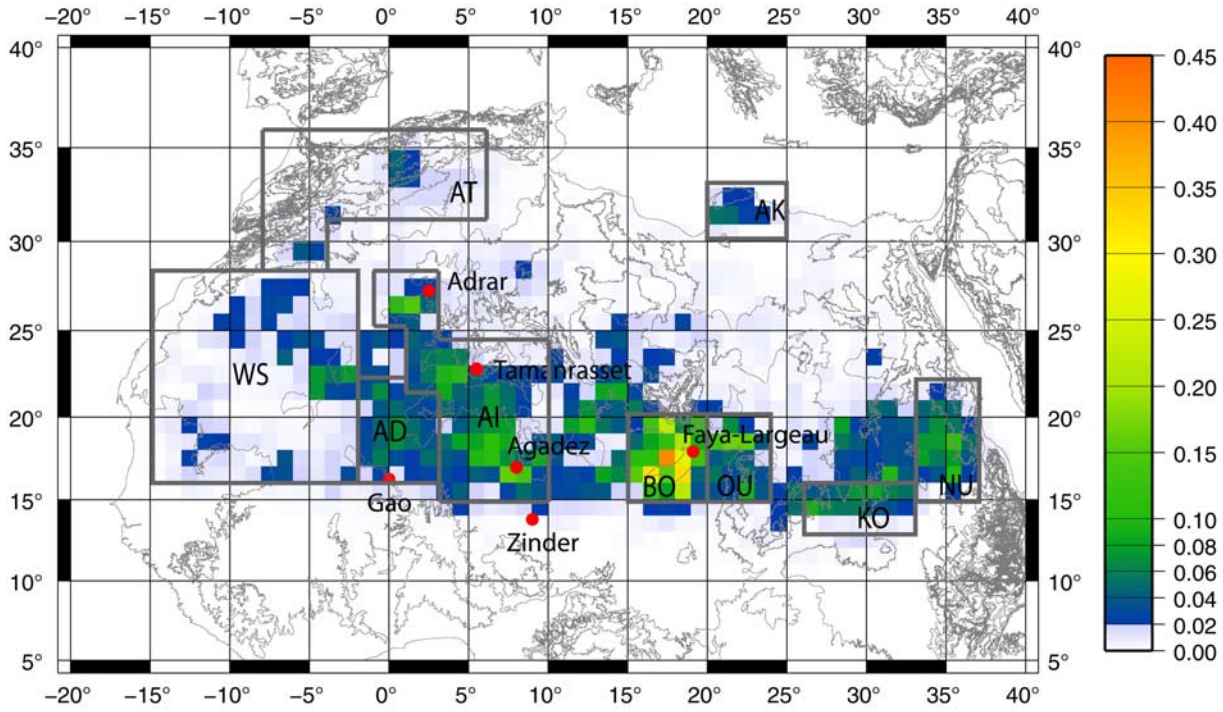

Figure 1. Fraction of dust source activations (DSA) per day during March 2006 to February 2008 except August 2007 derived from MSG IR dust index. High numbers of DSAs per day are observed in depression areas (Bodélé, sebkas, and chotts) and the foothills of the Saharan mountain areas. Red dots represent the location of synoptic stations considered in this study. The boxes mark the predefined subareas for discussion on the subdaily and monthly variability of observed DSA as shown in Figure 5. Topography indicated by contour lines at 250 m intervals is given by the GTOPO30 digital elevation data set provided by the U.S. Geological Survey.

from the first dust event has to occur. The inherent bias of the time-of-day distribution toward early times of the day does not affect the strong fraction of morning time dust source activations. DSAs downwind within a developing dust storm are not considered, and neither can dust sources totally covered by clouds. Currently the data set contains 2 years of observations between March 2006 and February 2008 (with August 2007 missing) with 3-h temporal resolution. The DSA therefore represents a frequency index for dust events, irrespective of their magnitude. It is the first available satellite based data set to provide information on the diurnal cycle of dust emission. For the Sahara we must emphasize that it is not a quantitative index of atmospheric dust burden. Instead it is a more direct measure of dust source activation and a more appropriate tool to study related emission processes compared to other satellite products based on retrievals at a single time of day. A detailed analysis of DSA in time and space (Figure 1) allows informed conjecture on the synoptic and mesoscale conditions likely to be forcing DSA.

3.2. Dust Source Analysis

3.2.1. Characteristics of Typical DSA Areas

[17] Most active dust source areas according to this data set are located in the foothills of the Saharan mountains (Figure 1). The areas are associated with endorheic water systems like wadis opening to alluvial fans, sebkhas and chotts in arid regions providing sediments due to fluvial abrasion, that can be lifted by strong winds [e.g., *Middleton and Goudie*, 2001; *Prospero et al.*, 2002; *Mahowald et al.*, 2003; *Zender and Newman*, 2003; *Engelstaedter et al.*, 2006; *Schepanski et al.*, 2007]. Dried out lake beds like the area of the paleolake Mega-Chad also provide fine sediments and can be efficient dust sources [*Goudie and Middleton*, 2001; *Prospero et al.*, 2002; *Mahowald et al.*, 2003]. Figure 2 shows the fraction of DSAs per day during 0300–0900 UTC representing the morning hours over the entire Saharan domain, and 1200–0000 UTC for the four seasons. Most DSAs occur during local morning hours in the Sahara (65% during 0600–0900 UTC, see Table 1), consistent with the pronounced diurnal cycle of LLJs and near surface winds (section 2.1). Indeed, the spatial patterns of DSAs (Figure 1) and especially those DSAs occurring in the morning hours are similar to that of LLJ frequencies in both the reanalysis (Figure 3) and LM-MUSCAT (Figures 3 and 4). A seasonal variability is evident as consequence of changing meteorological conditions. During winter (DJF) the Bodélé is the most frequently activated source area. Source activation is mainly during the morning hours by the breakdown of the Bodélé-LLJ (more than 30% of all days). In summer (JJA), the observed frequency of morning DSA increases over the Western Sahara compared to winter (DJF) and autumn (SON) to frequencies up to 20%. This is related to the West African Monsoon (WAM) circulation, which is identified to play a major role in forcing the nocturnal LLJ development over this area [e.g., *Parker et al.*, 2005;

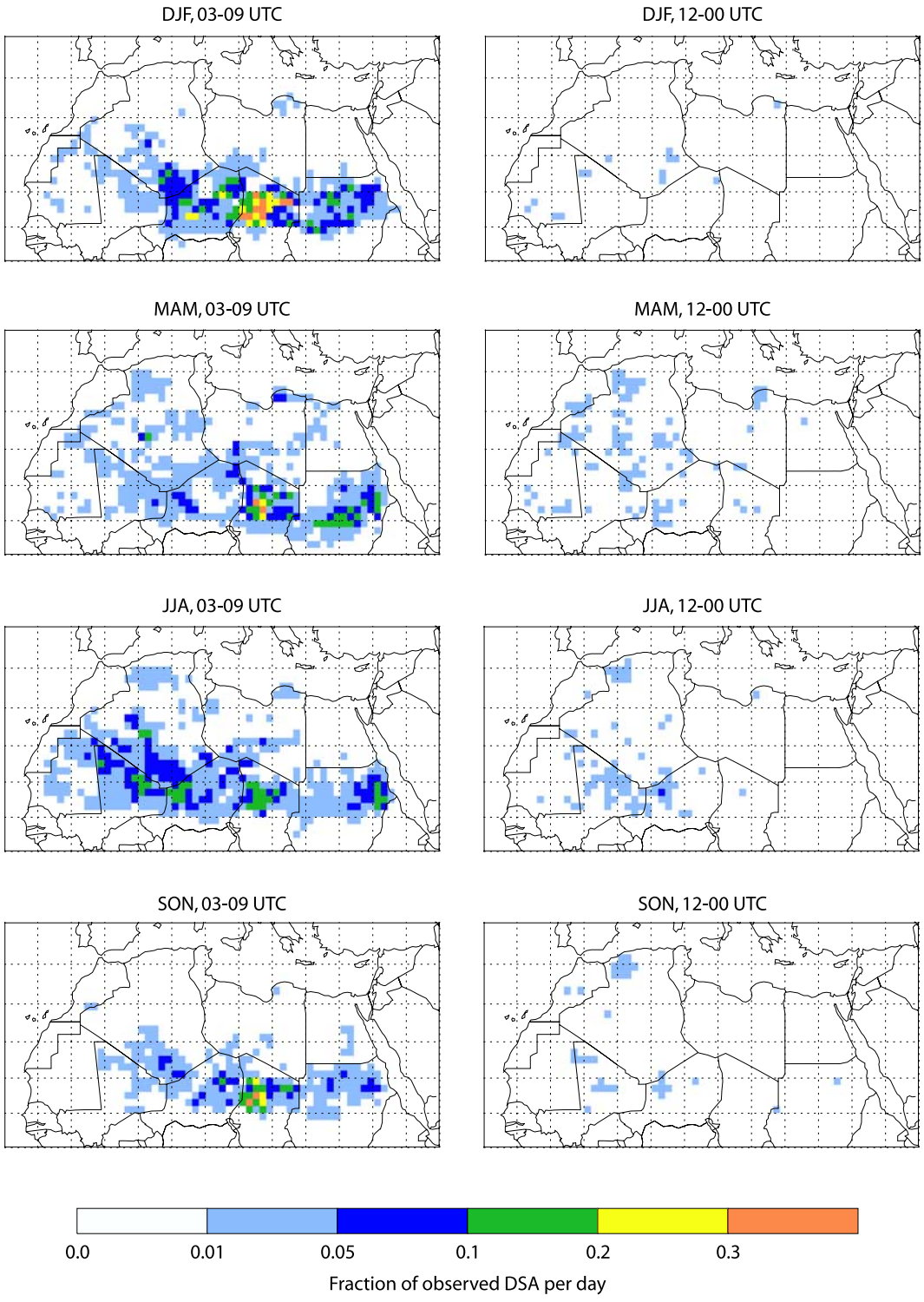

Figure 2. (left) Fraction of DSA per day for different seasons observed during 0300–0900 UTC (comprising local morning hours over the entire Saharan domain) and (right) seasonal fractions of dust source activations per day observed during 1200–0000 UTC. Morning time DSAs are mostly related to the breakdown of the nocturnal LLJ. Afternoon to night DSAs are mostly related to convective events.

Westphal et al., 1988]. In addition, the WAM provides moist air masses allowing deep moist convection to occur often resulting in strong density current gust fronts which can mobilize dust (haboobs). These features are most likely to occur in the local afternoon and nighttime [*Yang and Slingo*, 2001].

[18] Assuming that DSA related to moist convection mostly occurs between 1200 and 0000 UTC, the percentage

Table 1. Temporal Analysis of Frequent DSA Areas[a]

Time (UTC)	Total[b] (%)	Atlas (%)	Akhdar (%)	W-Sahara (%)	Air (%)	Adrar (%)	Bodélé (%)	Ouaddai (%)	Kordofan (%)	Nubia (%)
0000–0300	2	1	0	1	1	2	1	2	1	6
0300–0600	5	1	9	1	3	3	4	3	3	17
0600–0900	65	16	36	48	66	59	84	83	82	70
0900–1200	17	44	27	28	17	18	10	8	10	4
1200–1500	8	29	25	16	8	14	2	3	1	1
1500–1800	1	2	3	2	2	3	0	0	0	1
1800–2100	2	6	0	4	2	3	0	0	1	1
2100–0000	1	0	0	1	1	0	0	1	0	1

[a]As defined in section 3.2.1. Fraction of DSA observed per day within a 3-h period. Two-year period, March 2006 to February 2008.
[b]Total DSA observation area, northward of 5°N.

of DSA occurring during that time period may indicate the importance of convective cloud processes (Figure 2). The fraction of DSA observed during 1200–0000 UTC is low compared to fractions observed during 0300–0900 UTC. Nevertheless, a season-to-season variability of number of observed DSA per day of the 1200–0000 UTC time slot is evident. The percentage of DSA occurrence during 1200–0000 UTC is higher in the spring and summer seasons when convective cloud systems occur (up to 25% in April 2006), possibly associated with upper level disturbances due to troughs or moist convection during the monsoon period.

[19] Finally, in areas where the breakdown of the nocturnal LLJ plays a minor role for DSA, the percentage of 1200–0000 UTC DSA of the whole day DSAs can be more than 50% as it does for the Akhdar area. There, orographically induced clouds, upper level disturbances and density currents due to evaporation processes lead to wind speeds exceeding the threshold for DSA in mountain areas like the

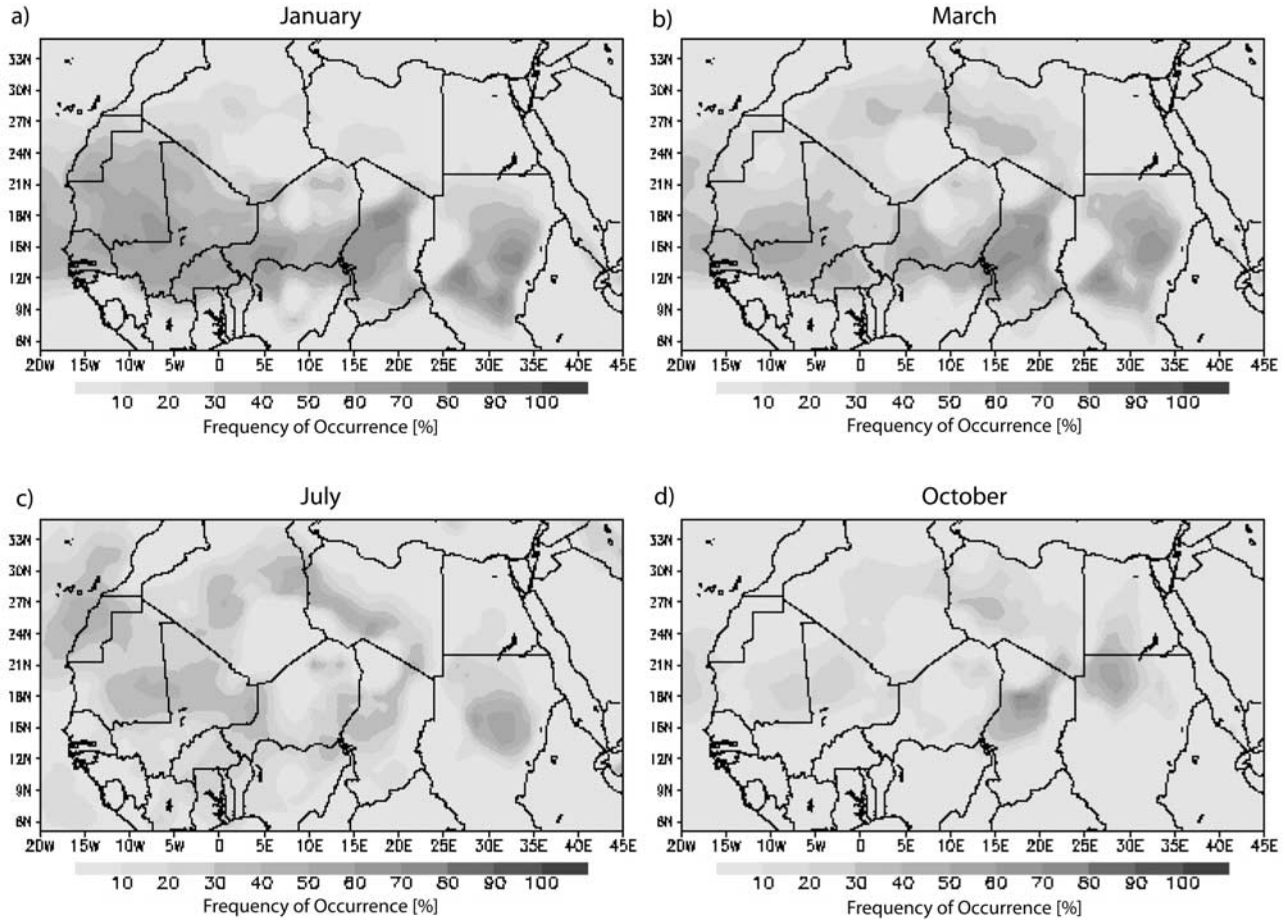

Figure 3. ERA-40 climatology: Frequency of LLJ ($\Delta v \geq 5$ m s^{-1} between 925 hPa and 770 hPa p level) during 10-year ERA-40 reanalysis (1990–1999) at 0600 UTC for (a) January, (b) March, (c) July, and (d) October.

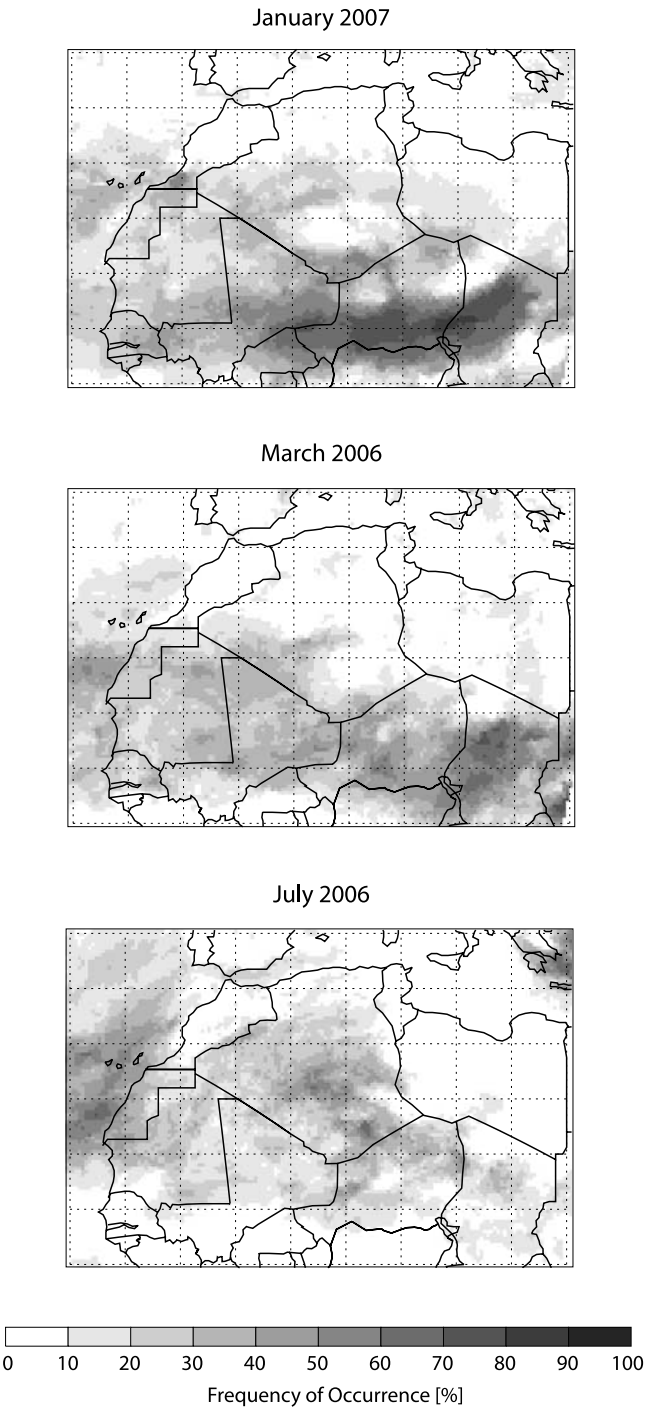

Figure 4. Frequency (%) of LLJ ($\Delta v \geq 5$ m s^{-1} between levels at around 925 hPa and 770 hPa) occurrence at 0600 UTC for January 2007, March 2006, and July 2006. The shown frequencies are computed from LM-MUSCAT model results.

Atlas during the afternoon and evening [*Knippertz et al.*, 2007, 2009].

[20] Areas with similar topographic conditions and DSA behavior are compiled into nine main DSA areas (Figure 1). These are the Atlas Mountains (AT, 82 grid cells), Akhdar Mountains (AK, 15 grid cells), Western Sahara (WS, 156 grid cells), Air Mountains (AI, 72 grid cells), Adrar Mountains (AD, 28 grid cells), Bodélé depression (BO, 25 grid cells), Ouaddai Mountains (OU, 20 grid cells), Kordofan (KO, 21 grid cells) and the Red Sea and Nubian Mountains (NU, 28 grid cells). Note that the defined areas have different sizes. The number of DSAs per month are not normalized to their size because of different distribution of local dust sources over the area. For example, in the Bodélé depression area, all grid cells are able to be a dust source, which is not the case for the Atlas area. Each area is characterized by specific topographical and meteorological conditions and provides fine sediment due to geomorphological surface processes. Major DSA areas show typical seasonal and diurnal patterns (Figure 5). In Table 1, time of day and frequency of DSA for the different predefined areas are listed. In the following, the seasonal and diurnal DSA patterns are described in detail for the individual regions.

3.2.2. Atlas Mountains

[21] The Atlas Mountains in northwestern Africa are situated like a barrier in the wind flow coming from the Atlantic ocean. Orographic clouds may develop during daytime reaching maximum in the afternoon. This is also the case for lee cyclones like the Sharav cyclone that develops especially in spring time. Both, orographic and baroclinic effects force strong surface wind speeds.

[22] DSA in the Atlas area is most frequent during spring (Figure 5). Besides a minimum during winter, a second maximum occurs in autumn (September and October) at least in 2008. LLJ frequency in the reanalysis data is relatively low and peaks during the summer months (Figure 6). In addition up to 30% of the dust mobilization events occur during the afternoon (Table 1) suggesting that the LLJ is not the dominant driver of dust emission in this region.

3.2.3. Akhdar Mountains

[23] The Akhdar Mountains located in the northeast of Libya with the Mediterranean Sea in the north and the Gulf of Sidra in the west are characterized by wadis and chotts on the Saharan side of the mountains. In the foothills on the Sahara side dust is most frequently activated during spring and early summer. Spring and early summer cyclones developing leeward of the Atlas move in eastward directions often cross the Libyan coast and cause strong wind speeds. Because of the thermal effect of insolation and heated surfaces, the development of cyclones occurs mostly during morning hours in the lee of the Atlas and reaches maximum during afternoon [*Trigo et al.*, 2002]. Moving eastward, the cyclones cross the Akhdar domain mostly during afternoon to evening hours.

[24] Besides DSA caused by cyclone activity, LLJs can develop and force high surface wind speeds in the vicinity of mountains situated parallel to the Mediterranean Sea but orthogonal to the coast to the Gulf of Sidra. As both processes are able to force DSA, time-of-day distribution of dust mobilization is variable, but morning hours (0600–0900 UTC) are dominant (Figure 5 and Table 1). The data shows a maximum occurrence of morning DSAs in winter and spring. However, as shown by the observations, the LLJ is not a very frequent phenomenon over the Akhdar area, indicated by relatively low total frequencies of occurrences (Figures 4 and 6).

3.2.4. Western Sahara

[25] In the Western Sahara, Ergs (dune fields, sand seas) and Hammadas (barren, rocky desert landscape) as well as

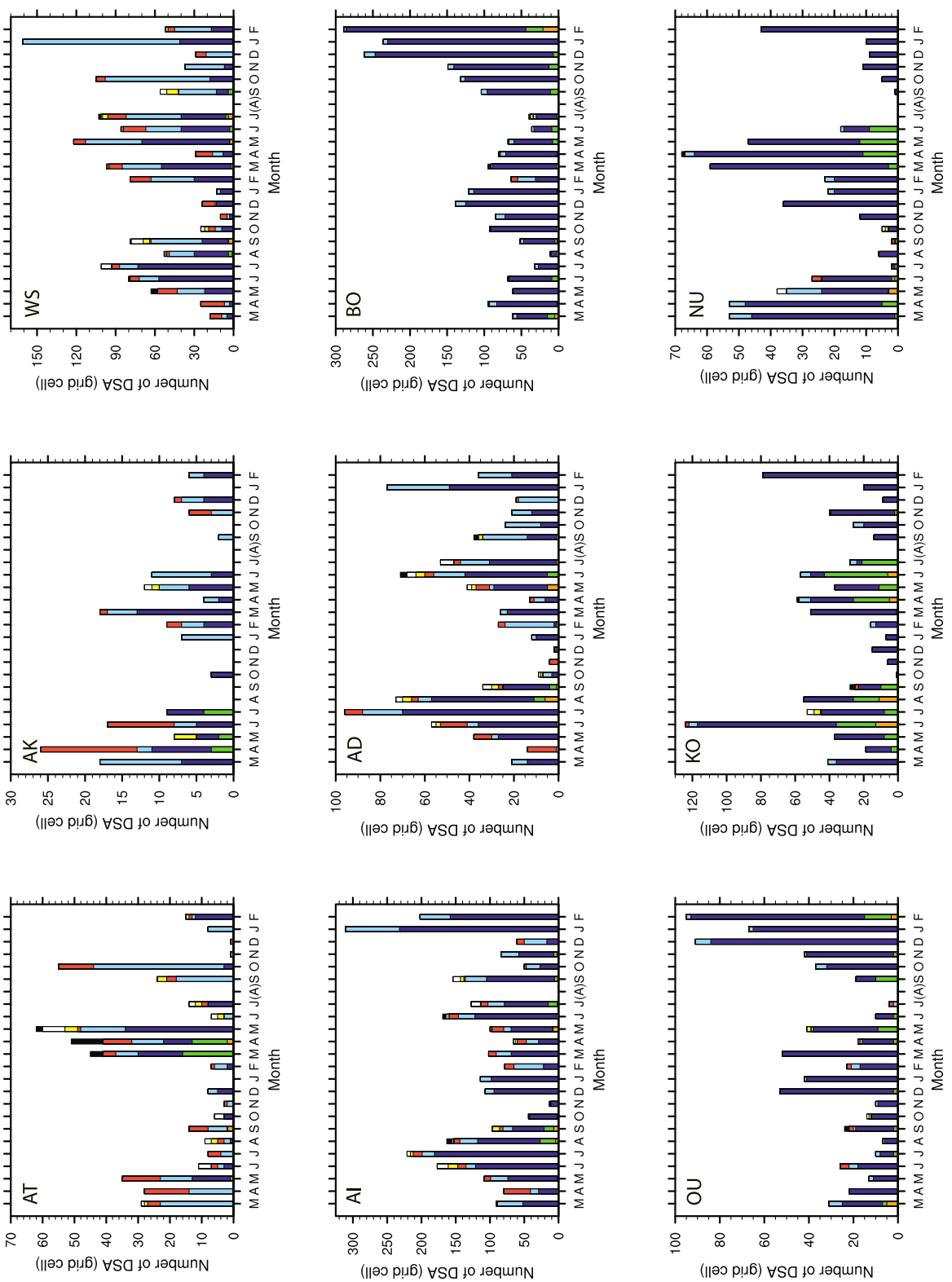
WS
BO
NU
AK
AD
KO
AT
AI
OU
Number of DSA (grid cell)
Month
M A M J J A S O N D J F M A M J J(A)S O N D J F

Figure 5

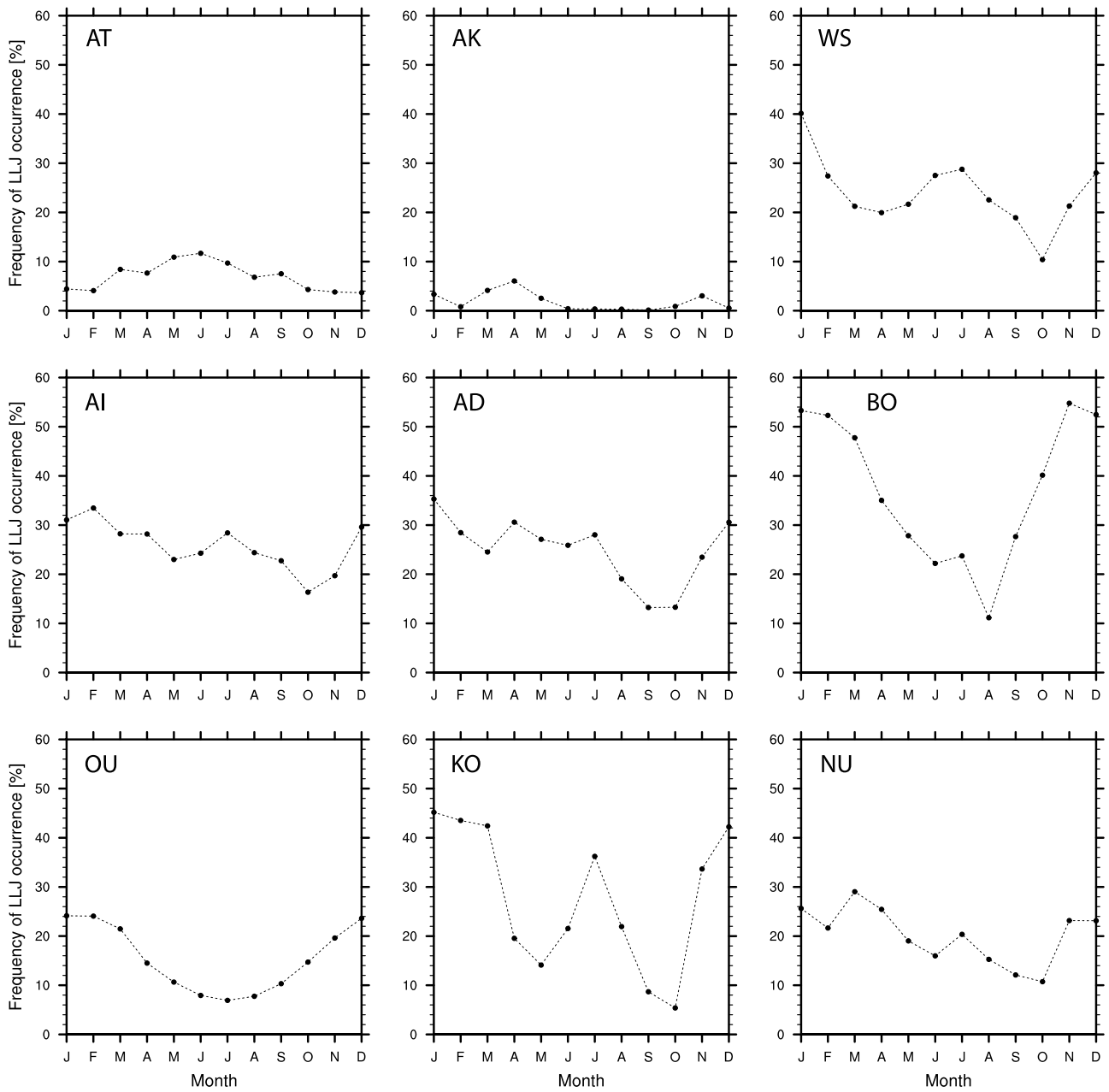

Figure 6. Spatiotemporal analysis of the frequency of LLJ occurrence ($\Delta v \geq 5$ m s^{-1} between 925 hPa and 770 hPa p level) over the defined areas, based on ERA-40 reanalysis data (1990–1999). The areas are defined following high fractions of observed DSAs per day. The Sahara is separated in nine areas: Atlas Mountains (AT), Akhdar Mountains (AK), Western Sahara (WS), Air Mountains (AI), Adrar Mountains (AD), Bodélé depression (BO), Ouaddai Mountains (OU), Kordofan (KO), and the Red Sea and Nubian Mountains (NU).

drainage systems and topographic gaps characterize the landscape. DSA is most frequent during summer (Figure 5), although there is variability in the annual cycle from year to year. In summer dust mobilization occurs at all times of the day, probably reflecting the occurrence of both (1) a mean midmorning peak in surface wind speeds associated with the downward mixing of the nocturnal LLJ (in both the Harmattan and monsoon circulations) and (2) density cur-

Figure 5. Spatiotemporal analysis of the Saharan dust source activation distribution for the observation period March 2006 to February 2008. Areas with high fractions of dust source activation (DSA) per day and characteristic topography or synoptic situations are analyzed concerning the frequency and time when DSA occurs. The Sahara is separated in the nine areas as shown in Figure 1. Colors are as follows: orange, 0000–0300 UTC; light green, 0300–0600 UTC; blue, 0600–0900 UTC; light blue, 0900–1200 UTC; red, 1200–1500 UTC; yellow, 1500–1800 UTC; white, 1800–2100 UTC; and black, 2100–0000 UTC. Note the different vertical scaling.

rents associated with convective clouds, which tend to peak in the afternoon and evening. During the morning hours, DSAs are common in all seasons (Figure 5). LLJ frequency in the reanalysis data (Figure 6) has a semiannual cycle with peaks in winter and summer suggesting that LLJs in the monsoon circulation may be more important than those in the Harmattan. During summer, a substantial proportion of DSA being triggered by deep moist convection, e.g., by density currents related to MCSs.

3.2.5. Adrar Mountains and Air Mountains

[26] Both the Adrar and Air Mountain areas show similar temporal pattern of number of DSA per month. For both areas the number of DSAs show a broad maximum during summer and a second narrow maximum in winter, although January and February 2008 were very active months. DSAs are most frequent during local morning hours between 0600 and 0900 UTC in all seasons (up to 100% of all DSA, see Figure 5). Both regions experience a high LLJ frequency with a semiannual cycle with peaks in winter and summer. This is consistent with the DSA distribution. The regions are also affected by ridges and troughs crossing in winter and spring time which can enhance the velocity of LLJs. The down-mixing of the LLJ momentum over potential dust source areas is a major cause for dust mobilization, especially in summer when under the influence of the WAM. However, downbursts originating form deep moist convection also occur in summer, which our results suggest play a likely secondary role for dust mobilization frequency.

3.2.6. Bodélé Depression and Ouaddai Mountains

[27] The Bodélé is the single most active dust source area of the world [e.g., *Prospero et al.*, 2002] and characterized by a minimum activity during summer months. The LLJ is stronger and more frequent over the Bodélé than over any other location in North Africa (Figures 4 and 6) and is most frequent in winter. The Bodélé is surrounded by the Tibesti Mountains to the north, the Ennedi Mountains in the northeast and the Ouaddai Mountains in the east. The mountains evidently affect the general wind flow by channeling the northeasterly LLJ especially during winter months. *Todd et al.* [2008] estimate from model experiments that topography is responsible for up to 50% of the peak LLJ wind speeds over the Bodélé. As the preconditions for wind acceleration due to channeling are often fulfilled, the LLJ develops frequently at night and forces high surface wind speeds the next day when turbulent mixing starts to mix momentum downward. Thus DSA in the Bodélé depression and the foothills of the adjacent mountains occurs very frequently after sunrise in the morning between 0600 and 0900 UTC (up to 85%). During summer months, a minimum of DSA occurs because of less frequent development of nocturnal LLJs (Figures 3 and 4) and lower mean wind speeds [*Todd et al.*, 2008]. This can be explained by the location of the intertropical discontinuity (ITD, conversion zone of the trade winds) related to weak geostrophic winds. Furthermore, during summer months wind direction is variable and topographic acceleration of air flow does not dominate.

[28] A strong seasonal cycle for DSA during the morning hours is observed (Figure 5 and Table 1) with a minimum in summer, especially in August. In addition, a strong amplitude between summer minimum and winter maximum is shown, pointing toward the importance of the LLJ in the seasonal cycle of DSA.

3.2.7. Kordofan

[29] The topography of the Kordofan in the northern Sudan is mainly characterized by the midaltitude Nubia Mountains with dense drainage channels like wadis likely to provide fluvial sediments. The hours between 0300 and 0900 UTC are again the most important time for DSA (see Figure 5 and Table 1), when solar heating starts and a convective BL develops which mixes the momentum of the nocturnal LLJs to the surface (up to 100% DSA before 0900 UTC). Note that local time here is UTC + 2 h, which explains the occurrence of DSA in the 0300–0600 UTC time slot. The annual cycle of DSA is not clear from the 2 years of DSA data although the absolute highest values occur in summer and winter month (Figure 5). This may be consistent with the relatively high frequency of LLJs in all months with peaks in summer and winter (Figure 6).

3.2.8. Nubian Region

[30] The area of high DSA in this region lies on the western foothills of the mountains, which separate the Nubian desert from the Red Sea. It is likely that sources of fine fluvial sediments are associated with wadis and endorheic drainage systems. Meteorological conditions force DSA mostly in spring and early summer. As for the Kordofan region to the south, the maximum number of DSA occurs in the morning hours (up to 100%) between 0300 and 0900 UTC (local time is UTC + 2 h). Again this indicates that the breakdown of the nocturnal LLJ may be the main mechanism to force DSA.

[31] In general, dust source areas located in the western part of the Sahara are most active during summer months, in contrast to those in the eastern part of the Sahara which are most active during winter and spring months. A predominance of dust sources activated during the morning hours indicate the likely important role of the breakdown of the nocturnal LLJ (e.g., Figures 2 and 5 and Table 1). In seasons with weak or absent nocturnal LLJ development the fraction of DSAs occurring during morning shows a minimum. DSAs at noon and afternoon are often associated with gusts related to deep moist convection. Mainly in the Atlas Mountains gusts related to orographic influence, orographic clouds, and density currents force DSA in afternoon hours.

[32] During winter (DJF) 2007/2008 DSAs occurred more frequently than during the same period 2006/2007. As DSA is mainly forced by atmospheric processes, detailed investigations of atmospheric conditions are necessary to explain this interannual variability and longer observation time series are required to decide whether the more recent high number of winter DSAs constitute an unusual condition.

4. LLJs and Surface Winds Over North Africa

[33] Occurrences of strong surface wind speeds are the main cause for dust mobilization. The dominance of satellite derived DSA during the morning hours (0600–0900 UTC) across the North African domain are an indication that the diurnal phase-lag relationship of LLJ and surface winds is an important mechanism for dust emission in the region. To understand this further and the connection with strong surface wind speeds causing dust mobilization, observed surface

Table 2. Monthly Median Wind Direction, Median Wind Speed of Wind Direction, and 75th Percentile of Wind Speed Measured at Adrar in 2006[a]

Time (UTC)	MAM (m s^{-1})	JJA (m s^{-1})	SON (m s^{-1})	Annual (m s^{-1})
0000	E 6.7 (9.3)	E 6.7 (7.2)	E 5.7 (8.7)	E 6.2 (8.2)
0300	E 6.7 (8.2)	E 6.7 (8.2)	E 5.7 (8.27)	E 8.2 (7.7)
0600	E 6.2 (7.2)	E 6.45 (7.7)	E 5.1 (7.7)	E 5.7 (7.7)
0900	E 9.3 (12.3)	SE 8.7 (11.3)	SE 6.95 (8.7)	E 8.7 (11.3)
1200	W 6.7 (10.3)	E 9.8 (12.3)	E 7.7 (10.3)	E 8.2 (10.3)
1500	W 11.05 (13.9)	E 8.7 (11.3)	NE 6.95 (10.8)	NE 6.7 (8.7)
1800	W 7.95 (9.3)	E 9.0 (10.3)	NE 6.2 (9.8)	NE 6.2 (8.2)
2100	NE 5.7 (6.2)	E 6.7 (7.7)	NE 5.1 (7.7)	E 5.1 (7.2)

[a]The 75th percentile of wind speed is given in parentheses. Adrar is located at 27°15′N, 2°31′E. MAM, March, April, and May; JJA, June, July, and August; SON, September, October, and November. Wind directions: N, north; E, east; S, south; W, west.

station reports, regional model and ERA-40 reanalysis data were analyzed.

4.1. Wind Observations at Synoptic Stations

[34] The observation of dust emission from remote sensing needs to be corroborated by ground measurements. Unfortunately, in the Sahara region the measurement network is sparse. Meteorological surface observation data are taken from the Integrated Surface Hourly (ISH) database (data set 3505 (DSI 3505)), provided by the National Climatic Data Center (NCDC), Asheville, NC, USA. Here, quality-checked synoptic weather observations of surface wind speed and direction (3-hourly) from stations in the Sahara/Sahel sector are analyzed. Only stations with an acceptable number of observations for statistical consideration are chosen.

[35] Results are shown for the stations Adrar (27°15′N, 2°31′E), Agadez (16°58′N, 7°59′E), Tamanrasset (22°47′N, 5°31′E), Gao (16°16′N, 0°03′W), Zinder (13°47′N, 8°59′E) and Faya-Largeau (17°56′N, 19°08′E), which have the most complete observation records. At other stations the numbers of observations at morning, especially between 0600 and 1200 UTC are too small to obtain meaningful results. Adrar is located westward of the Plateau de Tademait, Tamanrasset in the high Hoggar Mountains, Agadez in the southern foothills of the Air Mountains, Gao and Zinder in the Sahel/Savanna and Faya-Largeau to the North of the Bodélé depression (Figure 1). At some stations the suddenly increasing morning wind speeds are accompanied by a significant shift in wind directions. But at stations located in mountain areas close to mountain slopes, the wind direction may strongly be influenced by topography. However, all synoptic weather observations shown here indicate a significant increase in 10-m wind speeds during midmorning hours (Tables 2–4 and Figure 7). At most stations the observed 10-m wind speed decreases during noon and afternoon because of BL development, even at Adrar where mean wind speeds are higher. The mean diurnal cycle at these stations is consistent with the out of phase relationship between the diurnal cycle of the LLJ and surface winds described in section 2.1.

[36] The stations presented here are widely spread over the Sahara/Sahel sector indicating that the breakdown of the nocturnal LLJ, observed by increasing 10-m wind speeds, is a common phenomenon over North Africa.

4.2. Large-Scale Atmospheric Fields: ERA-40

[37] To complete the impression of the LLJ feature given by the station data, the occurrence of LLJ has been analyzed from 10 years (1990–1999) of the 40 year global atmospheric ERA-40 reanalysis fields provided by ECMWF [*Uppala et al.*, 2005]. The ERA-40 reanalysis data have a vertical resolution of 60 pressure levels up to 0.01 hPa and a horizontal resolution of 1° × 1° (T159). Wind speed was obtained at 6 hourly intervals over the 10-year period 1990–1999 and the magnitude of the vertical wind shear calculated from wind speeds at 925 hPa and 770 hPa. The existence of a LLJ was then determined with respect to a threshold wind shear of 5 m s^{-1}. The threshold is chosen with respect to vertical wind profiles performed for several representative locations. This analysis was conducted to (1) derive the spatial structure of LLJ frequency over the entire Sahara sector over an extended period of time, (2) to determine the annual cycle of LLJ frequency for defined areas of frequent dust source activation observed by MSG (see section 3.2.1), and (3) to determine whether a global atmospheric model on a coarse horizontal and vertical resolution is able to reproduce the meteorological feature of the nocturnal LLJ. Reanalysis fields have been used to derive dust emission fields [e.g., *Laurent et al.*, 2008], therefore the presence of this feature in ERA-40 reanalysis fields indicates to which extent ECMWF surface winds can

Table 3. Monthly Median Wind Direction, Median Wind Speed of Wind Direction, and 75th Percentile of Wind Speed Measured at Tamanrasset in 2006[a]

Time (UTC)	MAM (m s^{-1})	JJA (m s^{-1})	SON (m s^{-1})	Annual (m s^{-1})
0000	SE 3.1 (4.1)	E 3.1 (4.6)	E 3.6 (5.1)	E 3.6 (7.2)
0300	E 4.1 (5.7)	E 3.6 (6.7)	E 3.4 (5.7)	E 3.6 (8.2)
0600	E 4.1 (7.2)	E 4.1 (6.7)	E 4.1 (6.2)	E 4.1 (8.7)
0900	E 7.5 (9.3)	E 7.7 (9.8)	E 6.2 (7.7)	E 6.7 (11.3)
1200	SE 5.1 (7.2)	SE 6.2 (7.2)	S 4.1 (6.7)	SE 5.1 (9.3)
1500	NW 5.7 (7.2)	E 5.7 (7.7)	NW 4.1 (4.6)	NW 4.6 (8.7)
1800	NW 5.1 (7.2)	E 6.2 (6.2)	S 3.6 (4.6)	NW 4.6 (8.2)
2100	S 3.1 (3.6)	SE 3.1 (3.1)	SE 2.6 (3.1)	S 3.1 (5.1)

[a]The 75th percentile of wind speed is given in parentheses. Tamanrasset is located at 22°47′N, 5°31′E.

Table 4. Monthly Median Wind Direction, Median Wind Speed of Wind Direction, and 75th Percentile of Wind Speed Measured at Agadez in 2006[a]

Time (UTC)	MAM (m s^{-1})	JJA (m s^{-1})	SON (m s^{-1})	Annual (m s^{-1})
0000	E 4.1 (5.1)	E 3.1 (3.1)	E 2.1 (2.1)	E 3.1 (5.1)
0600	E 4.1 (5.1)	NW 2.6 (2.1)	E 2.1 (2.1)	E 4.1 (7.2)
0900	E 8.2 (11.8)	W 4.6 (5.1)	E 8.2 (8.7)	E 8.2 (11.8)
1200	E 8.2 (8.7)	NW 3.1 (4.1)	E 6.2 (8.2)	E 7.2 (11.8)
1500	E 5.1 (8.2)	SE 6.2 (6.2)	E 5.7 (7.2)	E 6.2 (9.8)
1800	SE 5.1 (6.2)	SE 5.1 (6.2)	SE 4.1 (5.1)	SE 4.1 (8.2)

[a]The 75th percentile of wind speed is given in parentheses. Agadez is located at 16°58′N, 007°59′E.

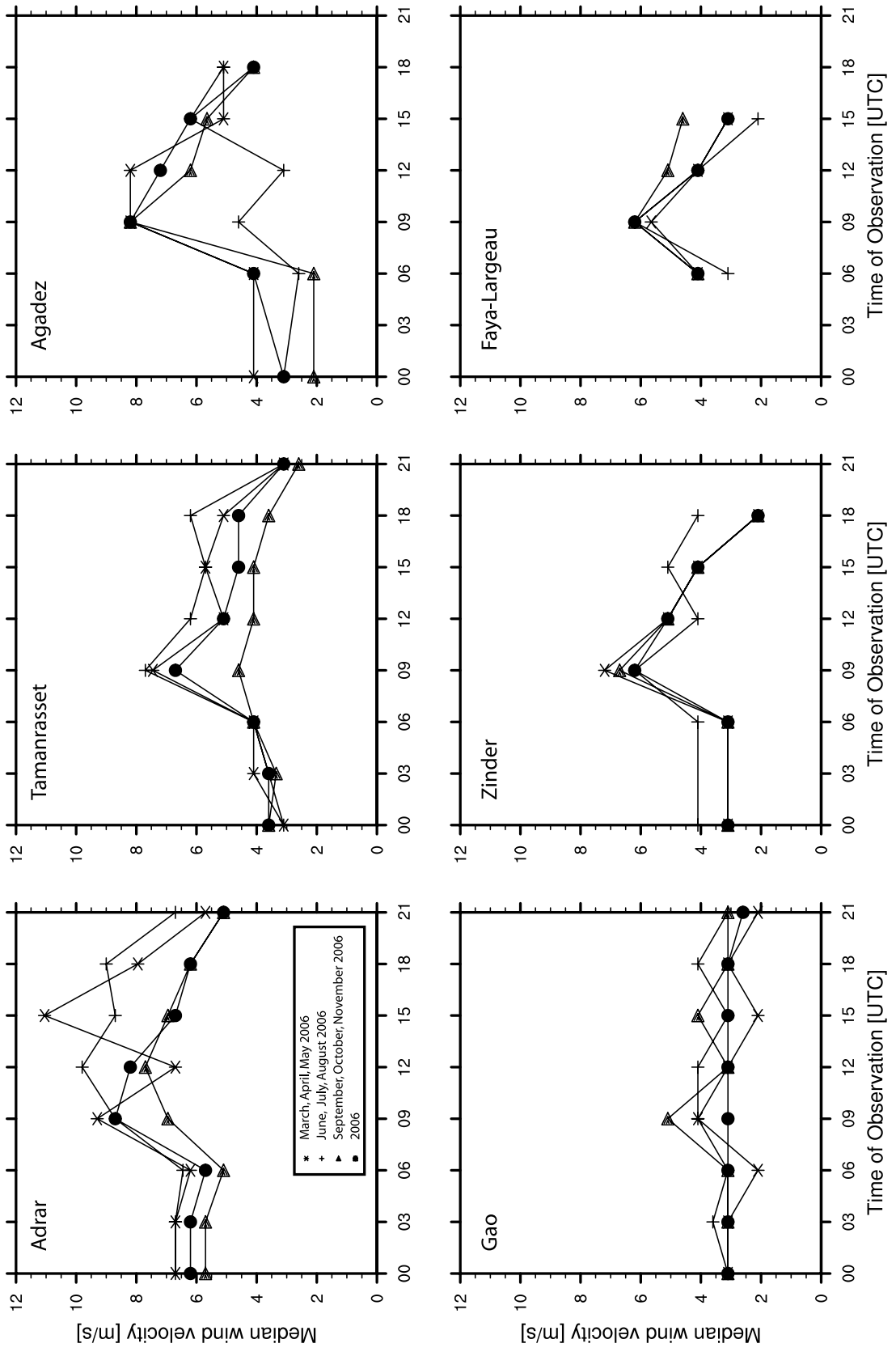

Figure 7. Median of observed wind speeds (m s^{-1}) for the seasons MAM (March, April, and May), JJA (June, July, and August), and SON (September, October, and November) 2006 at weather stations at Adrar (27°15′N, 2°31′E), Tamanrasset (22°47′N, 5°31′E), Agadez (16°58′N, 7°59′E), Gao (16°16′N, 0°03′W), Zinder (13°47′N, 8°59′E), and Faya-Largeau (17°56′N, 19°08′E).

Table 5. Comparison of the Seasonal Variability of the ERA-40 10-Year LLJ Occurrence Frequency and Observed Fraction of DSAs per Day for March 2006 to February 2008[a]

	DSA Observations			10-Year ERA-40			
Region	Seasonal Cycle	Maximum	Minimum	Seasonal Cycle	Maximum	Minimum	LLJ
Atlas (AT)	annual	MAM	DJF	weak, annual	DJF	JJA	not dominant
Akhdar (AK)	annual	MAM	SON	weak, annual	MAM	JJA	not dominant
W-Sahara (WS)	semiannual	JJA, DJF	MAM, SON	semiannual	JJA, DJF	MAM, SON	important
Air (AI)	semiannual	JJA, DJF	SON	weak, semiannual	JJA, DJF	SON	important
Adrar (AD)	semiannual	JJA, DJF	SON	semiannual	DJF, JJA	SON	important
Bodélé (BO)	annual	DJF	JJA	annual	DJF	JJA	dominant
Ouaddai (OU)	annual	DJF	JJA	annual	DJF	JJA	dominant
Kordofan (KO)	annual	JJA	SON	semiannual	DJF, JJA	MAM, SON	dominant
Nubia (NU)	annual	MAM	SON	annual	MAM	SON	important

[a]See also Figures 5 and 6 for comparison. "Semiannual" seasonal cycle indicates the presence of a secondary maximum in LLJ and/or DSA. DJF, December, January, and February (winter); MAM, March, April, and May (spring); JJA, June, July, and August (summer); SON, September, October, and November (autumn).

represent the meteorological situation responsible for a large number of dust emission events in the Sahara.

[38] While the vertical and temporal resolution of the ERA-40 data is not always sufficient to resolve the fine detail of LLJ features [*Todd et al.*, 2008] the data provide a good representation at the larger scale. However, it should be noted that the ERA-40 data are based on pressure levels, such that the data might not be able to represent the low-level atmosphere over high mountain regions which are dominant in this analyzed domain.

4.2.1. Ten-Year LLJ Climatology

[39] The mean frequency of nocturnal LLJs represented by the 0600 UTC low-level wind shear in ERA-40 data is shown in Figure 3. During the winter (Figure 3a) LLJs are widespread across the Sahel and southern Sahara occurring on 50% of nights in a broad zone between 10–20°N extending almost the entire longitudinal extent of the continent. These LLJs occur within the mean northeasterly low-level flow (the "harmattan") which dominates North Africa in winter. LLJ frequency and magnitude is greatest where the large-scale flow is influenced by topography, notably downwind of the Tibesti-Ennedi gap over the Bodélé depression of northern Chad, south of the Air Mountains in central Niger and to the west of the Ethiopian Highlands in eastern Sudan. During summer (Figure 3c) LLJ frequency is lower (by about 30–40%) over the continent and the main axis shifts northward such that the occurrence is focussed between about 15 and 30°N. This region encompasses the mean position of summer intertropical discontinuity, the divide between the dry northeasterly flow and the moist southwesterly monsoon flow. As such, nocturnal LLJ features occur in both circulations. While it is clear that LLJs are enhanced close to regions of pronounced topography, it should be borne in mind that the results shown in Figure 3 are based on pressure level data, such that they do not represent the low-level atmosphere over regions of high surface elevation. Satellite based data sets, however, indicate dust emission directly over mountain foothills, where wadis and drainage systems provide lot of fine, fluvial sediments [e.g., *Washington et al.*, 2003; *Schepanski et al.*, 2007].

4.2.2. ERA-40 10-Year LLJ for Defined Regions

[40] The mean seasonal cycle of LLJ occurrence in ERA-40 data for the key dust source regions (defined from analysis of the satellite DSA data, see Figure 1 and section 3.2.1) are shown in Figure 6. Over some areas, a weak seasonal cycle is shown by the ERA-40 analysis, e.g., the Atlas, and the Akhdar, whereby the observed number of DSAs during the morning hours show a stronger season-to-season variability. Generally, two different types of seasonal variability are evident following a semiannual or an annual cycle depending on the seasonality of atmospheric circulation patterns forcing the LLJ development. The Bodélé and the Ouaddai region for example show a strong winter maximum. Over the West Sahara, a second maximum during summer is evident, likely related to the forcing of the nocturnal LLJ development by the WAM [*Parker et al.*, 2005]. In the Atlas and Akhdar regions indicate the LLJ is a less important phenomenon shown by low occurrence frequencies retrieved from ERA-40 reanalysis (Figure 6). It is interesting to note that the seasonal cycle of number distribution of DSAs shows similar seasonal characteristics to the LLJ in the reanalysis data for most regions (Table 5). This points toward the important role of the LLJ for DSA over these areas, an issue which has been developed further in section 3.2.1.

4.3. Regional Model LM-MUSCAT

[41] The analysis in section 4.2.2 shows the widespread occurrence of LLJ phenomena in the reanalysis data and the relationship with DSA. In the following section the linkage of LLJ breakdown and dust mobilization will be investigated using a regional-scale model in addition to the large-scale reanalysis. The role of LLJs in forcing DSA is demonstrated by the regional dust emission and transport model LM-MUSCAT [*Heinold et al.*, 2007]. The model consists of the meteorological regional model Lokal-Modell (LM) provided by the German Weather Service, Deutscher Wetterdienst (DWD) [*Steppler et al.*, 2003], and the Multi-Scale Chemical Aerosol Transport Model (MUSCAT [*Wolke et al.*, 2004a, 2004b]), including a dust emission scheme based on work by [*Tegen et al.*, 2002]. Dust emission, transport and deposition are simulated with MUSCAT using meteorological and hydrological fields that are computed by the LM and updated every advection time step comprising two LM time steps of 80 s. Local wind systems, clouds, precipitation, and mesoscale convection are simulated depending on topography. Subgrid-scale moist convection is parameterized following [*Tiedtke*, 1989].

[42] Soil erosion by wind mostly depends on the wind shear stress on the ground and occurs when the surface friction velocity increases above the threshold friction velocity, itself dependent on soil conditions of aerodynamic and smooth roughness length, and dry soil size distribution. Dust emission fluxes are computed using LM surface winds and soil moisture. In this study, dust emission in the model is only allowed for areas where dust source activation is observed on at least 2 days per year by the MSG-SEVIRI IR dust index during the observation period March 2006 to February 2007. Mobilized dust is transported as passive tracer in five independent size classes with radius limits at 0.1 μm, 0.3 μm, 0.9 μm, 2.6 μm, 8 μm, and 24 μm [*Heinold et al.*, 2007, 2009].

[43] The model simulations were performed for an area covering 0.2°N, 32.3°W to 41.3°N, 33.3°E with a horizontal resolution of 28 km and 40 vertical layers. For analyzing meteorological conditions able to force dust mobilization, three case studies in different seasons have been computed: March 2006, July 2006, and 20 December 2006 to 20 January 2007 (hereafter January 2007).

4.3.1. LLJ Occurrence and Dust Mobilization: Regional Modeling Study

[44] The breakdown of the LLJ provides high surface wind speeds suitable for dust mobilization. Here, the regional model system LM-MUSCAT is used to show the relation between LLJ occurrence and dust emission. For a more detailed description of the atmospheric conditions vertical distribution of horizontal wind, potential temperature, gradient Richardson number and the surface dust emission flux is presented for the location of Agadez (a key dust location for) for March 2006 (Figure 8). The gradient Richardson number *Ri* denotes the ratio of stability to wind shear and can be used as indicator for turbulent processes [*Reiter and Lester*, 1968] and is assumed for $Ri \leq Ri_c$, the critical value. Turbulence occurs for $Ri_c = 1$, in weakly stratified layers for $Ri_c = 0.25$ [e.g., *Sorbjan*, 2006].

[45] During night, the lower troposphere is stably stratified. Weak shear indicated by positive *Ri* numbers dominates and no turbulence occurs. Surface wind speeds are too low for dust mobilization. Because of frictional decoupling of air aloft supergeostrophic conditions develop at around 1 km. Hence, air aloft accelerates and a LLJ develops. Before sunrise, wind shear increases because of the LLJ but atmospheric stability still suppresses turbulence occurrence. Soon after sunrise surface heats up and air masses at near-surface levels become unstable. The *Ri* number decreases, changes sign indicating unstable conditions and turbulent mixing starts. The layer of unstable conditions grow up with increasing surface heating. At 0800 UTC, the unstable layer depth reaches height of the nocturnal LLJ. Momentum from the LLJ is mixed down leading to suddenly increasing wind speeds, up to 10 m s^{-1} on 19 March 2006 (Figure 8). These wind speeds are high enough to cause dust emission. At noon, a well mixed boundary layer is developed, characterized by a homogeneous distribution of potential temperature, horizontal wind speed, and large, negative *Ri* numbers. Subgeostrophic conditions occur because of frictional coupling of the boundary layer to the surface.

[46] Considering the whole month (here March 2006, shown in Figure 8), the LLJ occurs on almost all nights. Enhanced LLJ development occurred during 7–11 March, 18–21 March, and 25–28 March when dust emission occurred associated with anomalous high-pressure ridges over North Africa. The dust event of 7–11 March is particularly notable [*Milton et al.*, 2008; *Tulet et al.*, 2008].

[47] The different time-of-day distribution of near-surface (first-layer, around 33 m above ground level (agl)) wind speeds on days with LLJ development (LLJ days) and days without LLJ development is evident in the median wind speed distribution for both modeling results and synoptic observations (Figure 9) shown at Agadez. On LLJ days, the wind speed increases suddenly at around 0800 UTC and decreases during the afternoon hours. During night, the wind speeds are lower than the threshold for dust emission (see Figure 8). Differences between model results and synoptic observations are evident. In the LLJ case, the observed wind speed peaks around 2 h earlier than the simulated. This is likely to be related to inadequacies in the planetary boundary layer scheme [*Todd et al.*, 2008]. Furthermore, the height difference between 10-m wind measurements and model results given for the first model layer leads to an offset for the simulated wind speed. Nevertheless, the magnitude of observed wind speeds are in a good agreement with the simulated wind speeds. On days without LLJ development, both model results and observations indicate low wind speeds. The LM-MUSCAT simulations indicate the importance mixing down the LLJ to produce high near surface wind speeds necessary for dust emission. To put these results in regional context, the local nocturnal LLJ occurrence frequency in the regional model is computed for the Sahara for different months (Figure 4). Nocturnal LLJ conditions are assumed if the wind speed difference Δv between 925 hPa and wind speed at 770 hPa exceeds 5 m s^{-1}. The threshold of 5 m s^{-1} for Δv is empirically obtained by analyzing vertical profiles and allows to capture most of the LLJs. Single cyclonic disturbances over the Atlas and especially over the Mediterranean Sea and Southern Europe can also fulfill the conditions indicating LLJs because of their vertical wind speed profile. In Figure 4, the frequency of LLJ occurrence ($\Delta v \geq 5$ m s^{-1}) at 0600 UTC is shown for atmospheric winter conditions in January 2007 (20 December 2006 to 20 January 2007), for March 2006 representing atmospheric spring conditions and for July 2006 representing atmospheric summer conditions. The distribution as well as the frequency of LLJ occurrence change with season. During winter and spring, the Bodélé depression is characterized by a very high frequency of LLJ occurrence (up to 90% and more). In January, a band-like pattern of high frequencies (over 80%) occurs over the Sahel and South Sahara, which is the area where the LLJ is the most dominant. Further more north, the gap between the Tassili of Ajjer (directly north to the Hoggar) and the Tibesti show high LLJ frequencies as well (up to 75%). Besides the regions proximate to the Saharan highlands, LLJs over the Ergs in the Western Sahara occur with a moderate frequency around 50–60%. Over the Atlas and north Algeria, the LLJ frequency is low, mostly lower than 10%. In spring, besides the dominant LLJ feature over the Bodélé depression, additional areas characterized by high frequencies of nocturnal LLJ occurrence are the sebkhas and ergs over the Western Sahara with frequencies between 50 and 60% as well as the Akhdar Mountains (around 50%). In July 2006 the areas of high frequencies are mainly the central and

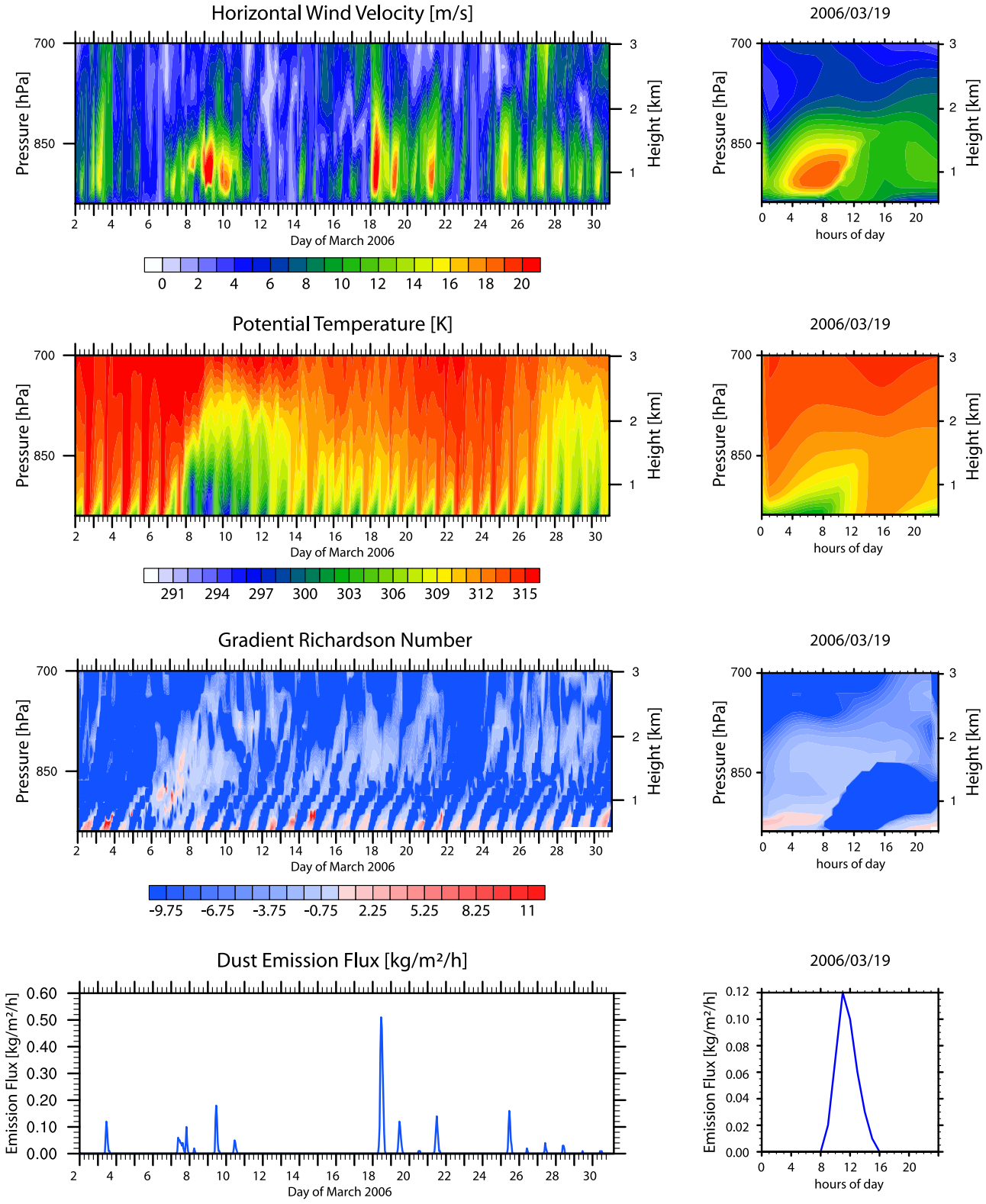

Figure 8. Time series of the vertical distribution of horizontal wind speed (m s^{-1}), potential temperature (K), Richardson number, and dust emission flux (kg m^{-2} h^{-1}) at Agadez (16°58′N, 7°59′E) (left) for the month of March 2006 and (right) exemplary for 19 March 2006. The time series are taken from model results using LM-MUSCAT.

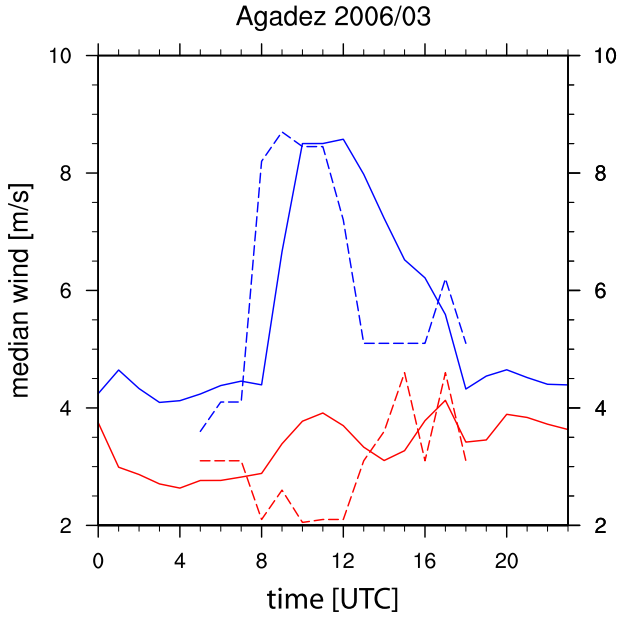

Figure 9. Median wind speed for March 2006 at Agadez (16°58′N, 7°59′E). Solid lines show first layer wind simulations by the LM-MUSCAT, and dashed lines show synoptic observations of 10-m winds. On the basis of the occurrence of low-level wind speed maxima shown in Figure 8, days are separated in LLJ days (top pair of blue curves) and days without LLJ development (bottom pair of red curves).

south Algerian mountains (up to 80%) and mountains in Niger (up to 60%).

[48] Both the major patterns of high frequency in January 2007 and March 2006 computed with the regional model agree well with the 10-year climatology derived from the global atmospheric ERA-40 reanalysis fields (Figure 3). Differences between regional and global fields are likely to be related to different horizontal and vertical resolutions, and thereby to different representations of subgrid-scale features and topography, and to different parameterizations of surface and boundary layer processes. Overall, regional and global models are able to simulate a similar structure of LLJ occurrence which is consistent with the spatiotemporal pattern of satellite based DSA.

5. Conclusion

[49] This study presents the first comprehensive study of the diurnal characteristics of dust storm activation (DSA), based on a new data set derived from MSG-SEVIRI satellite data. The high temporal resolution of the SEVIRI data ensures that the DSA data set resolves the diurnal cycle of dust and allows backtracking of dust plumes directly to source regions. In this way the fraction of DSA per day is much more closely related to processes of dust emission than other satellite data sets, which provide some estimate of column integrated dust burden. The DSA data set of the Sahara based on 15 min MSG IR dust index retrievals is used to show the spatial and temporal distribution of DSA over the period of 2 years. The results here show that DSA in the Sahara is most commonly observed in the local early morning hours after sunrise. Such a condition can be explained by the first-order phase-lagged relationship between the nocturnal LLJ and surface winds. The downward mixing of nocturnal LLJs by turbulent mixing of momentum after sunrise leads to peak surface wind speeds and dust emission in the hours after sunrise. We can infer that this may be a dominant mechanism for DSA in the Sahara. The arid and stable climate over the Saharan desert provide preconditions for the development of nocturnal LLJs, which are a widespread phenomenon across the region. DSA is most commonly observed close to the mountain regions of the Sahara. We speculate that this is due to a combination of the accumulation of fine sediments from fluvial erosion processes and the high frequency of LLJ occurrence in those regions. Model experiments with LM-MUSCAT confirm that the breakdown of the LLJ can lead to dust emission. These dust events are generally associated with synoptic-scale variability resulting in large-scale forcing of low-level and surface wind speeds. As such, it is the combination of the mean diurnal cycle in low-level and surface winds with the day-to-day synoptic-scale variability that explains much of the variability at diurnal time scales.

[50] Of course there are many other meteorological conditions that lead to dust emission and some of these have been highlighted by the analysis of DSA. These include (1) downbursts associated to moist convective dynamics during the monsoon period, (2) orographic forced gusts due to orographic clouds and blocking situations, and (3) cyclonic activity (mainly the Sharav cyclones during spring time over North Africa). For a comprehensive understanding detailed investigations on summer meteorological conditions, especially in context of the WAM, remain necessary.

[51] The MSG-based analysis of DSA gives only information on the frequency of source activity, not on the strength of such sources. To clarify the role of LLJ for total dust emission fluxes, quantitative dust retrievals over desert surface are needed.

[52] Furthermore, the statistical analysis of DSAs shows a clear interannual variability. To explain this variability, longer time series and detailed investigations concerning interannual variability of major atmospheric conditions will be performed in the future.

[53] **Acknowledgments.** We thank the Deutscher Wetterdienst (DWD) for good cooperation and support. We also thank the U.S. Geological Survey's Earth Resources Observation and Science (EROS) data center for providing GTOPO30 digital elevation data set, available at http://www.edc.usgs.gov. Furthermore, we thank the anonymous reviewers for their helpful suggestions to improve the manuscript.

References

Alpert, P., and B. Ziv (1989), The Sharav Cyclone: Observations and some theoretical considerations, *J. Geophys. Res.*, *94*, 18,495–18,514.

Alpert, P., B. I. Neeman, and Y. Shay-el (1990), Climatological analysis of Mediterranean cyclones using ECMWF data, *Tellus, Ser. A*, *42*, 65–77.

Banta, R. M., R. K. Newsom, J. K. Lundquist, Y. L. Pichugina, R. L. Coulter, and L. J. Mahrt (2002), Nocturnal low-level jet characteristics over Kansas during CASES-99, *Boundary Layer Meteorol.*, *105*, 221–252.

Banta, R., Y. L. Pichugina, and R. K. Newson (2003), Realtionship between low-level jet properties and turbulence kinetic energy in the nocturnal stable boundary layer, *J. Atmos. Sci.*, *60*, 2549–2555.

Banta, R. M., Y. L. Pichugina, and W. A. Brewer (2006), Turbulent velocity-variance profiles in the stable boundary layer generated by a nocturnal low-level jet, *J. Atmos. Sci.*, *63*, 2700–2719.

Barkan, J., P. Alpert, H. Kutiel, and P. Kishcha (2005), Synoptics of dust transportation day from Africa toward Italy and central Europe, *J. Geophys. Res.*, *110*, D07208, doi:10.1029/2004JD005222.

Blackadar, A. K. (1957), Boundary layer wind maxima and their significance for the growth of nocturnal inversion, *Bull. Am. Meteorol. Soc.*, *38*(5), 283–290.

Bou Karam, D., C. Flamant, P. Knippertz, O. Reitebuch, J. Pelon, M. Chong, and A. Dabas (2008), Dust emission over the Sahel associated with the West African monsoon inter-tropical discontinuity region: A representative case study, *Q. J. R. Meteorol. Soc.*, *134*(632), 621–634, doi:10.1002/qj.244.

Brooks, N., and M. Legrand (2000), Dust variability over northern Africa and rainfall in the Sahel, in *Linking Climate Change to Landsurface Change*, edited by S. J. McLaren and D. Kniveton, pp. 1–25, Kluwer Acad, Dordecht, Netherlands.

Charba, J. (1974), Application of gravity current model to analysis of squall-line gust front, *Mon. Weather Rev.*, *102*, 140–156.

Claquin, T., M. Schulz, and Y. J. Balkanski (1999), Modeling the mineralogy of atmospheric dust sources, *J. Geophys. Res.*, *104*(D18), 22,243–22,256.

Davis, P. A. (2000), Development and mechanisms of the nocturnal jet, *Meteorol. Appl.*, *7*(3), 239–246.

Dayan, U., J. Heffter, J. Miller, and G. Gutman (1991), Dust intrusion into the Mediterranean Basin, *J. Appl. Meteorol.*, *30*, 1185–1199.

Droegemeier, K. K., and R. B. Wilhelmso (1987), Numerical simulation of thunderstom outflow dynamics. Part I: Outflow sensitivity experiments and turbulence dynamics, *J. Atmos. Sci.*, *44*(8), 1180–1210.

Egger, J., P. Alpert, A. Tafferner, and B. Ziv (1995), Numerical experiments on the genesis of Sharav cyclones: Idealized simulations, *Tellus, Ser. A*, *47*(2), 162–174.

Engelstaedter, S., and R. Washington (2007), Atmospheric controls on the annual cycle of North African dust, *J. Geophys. Res.*, *112*, D03103, doi:10.1029/2006JD007195.

Engelstaedter, S., I. Tegen, and R. Washington (2006), North African dust emission and transport, *Earth Sci. Rev.*, *79*, 73–100, doi:10.1016/j.erscirev.2006.06.004.

Flamant, C., J.-P. Chaboureau, D. J. Parker, C. M. Taylor, J.-P. Cammas, O. Bock, F. Timouk, and J. Pelon (2007), Airborne observations of the impact of a convective system on the planetary boundary layer thermodynamics and aerosol distsribution in the inter-tropical discontinuity region of the West African monsoon, *Q. J. R. Meteorol. Soc.*, *133*, 1175–1189, doi:10.1002/qj.97.

Fung, I., S. Meyn, I. Tegen, S. C. Doney, J. John, and J. K. B. Bishop (2000), Iron supply and demond in the upper ocean, *Global Biogeochem. Cycles*, *14*, 281–296.

Garratt, J. R. (1992), *The Atmospheric Boundary Layer*, Cambridge Univ. Press, Cambridge, U. K.

Ginoux, P., M. Chin, I. Tegen, J. M. Prospero, B. Holben, O. Dubovik, and S.-J. Lin (2001), Sources and distributions of dust aerosols simulated with the GOCART model, *J. Geophys. Res.*, *106*(D17), 20,255–20,273.

Goudie, A. S., and N. J. Middleton (2001), Saharan dust storms: Nature and consequences, *Earth Sci. Rev.*, *56*, 179–204.

Heinold, B., J. Helmert, O. Hellmuth, R. Wolke, A. Ansmann, B. Marticorena, B. Laurent, and I. Tegen (2007), Regional modeling of Saharan dust events using LM-MUSCAT: Model description and case studies, *J. Geophys. Res.*, *112*, D11204, doi:10.1029/2006JD007443.

Heinold, B., et al. (2009), Regional Saharan dust modelling during the SAMUM 2006 campaign, *Tellus, Ser. B*, *61*(1), 307–324, doi:10.1111/j.1600-0889.2008.00387.x.

Herman, J. R., P. K. Bhartia, O. Torres, C. Hsu, C. Seftor, and E. Celarier (1997), Global distribution of UV-absorbing aerosols from Nimbus 7/TOMS data, *J. Geophys. Res.*, *102*(D14), 16,922–16,922.

Holton, J. R. (1967), The diurnal boundary layer wind oscillation above sloping terrain, *Tellus*, *19*(2), 199–205.

Horvath, K., L. Fita, R. Romero, and B. Ivančan-Picek (2006), A numerical study of the first phase of a deep Mediterranean cyclone: Cyclogenesis in the lee of the Atlas Mountains, *Meteorol. Z.*, *15*(2), 133–146, doi:10.1127/0941-2948/2006/0113.

Hoxit, L. R. (1975), Diurnal variations in planetary boundary-layer winds over land, *Boundary Layer Meteorol.*, *8*, 21–38.

Hsu, N. C., S. C. Tsay, M. D. King, and J. R. Herman (2004), Aerosol properties over bright-reflecting source regions, *IEEE Trans. Geosci. Remote Sens.*, *42*(3), 557–569.

Idso, S. B., R. S. Ingram, and J. M. Pritchard (1972), An American haboob, *Bull. Am. Meteorol. Soc.*, *53*(10), 930–935.

Intergovernmental Panel on Climate Change (2007), *Climate Change 2007: The Physical Science Basis—Contribution of Working Group I to the Fourth Assessment Report of the Intergovernmental Panel on Climate Change*, edited by S. Solomon et al., Cambridge Univ. Press, Cambridge, U. K.

Jickells, T. D., et al. (2005), Global iron connections between desert dust, ocean biogeochemistry, and climate, *Science*, *308*(5718), 67–71.

Knippertz, P., and J. E. Martin (2005), Tropical plumes and extreme precipitation in subtropical and tropical West Africa, *Q. J. R. Meteorol. Soc.*, *112*, 2337–2776.

Knippertz, P., C. Deutscher, K. Kandler, K. Müller, T. Schulz, and L. Schütz (2007), Dust mobilization due to density currents in the Atlas region: Observations from the SAMUM 2006 field campaign, *J. Geophys. Res.*, *112*, D21109, doi:10.1029/2007JD008774.

Knippertz, P., et al. (2009), Dust mobilization and transport in the northern Sahara during SAMUM 2006—A meteorological overview, *Tellus, Ser. B*, *61*(1), 12–31, doi:10.1111/j.1600-0889.2008.00380.x.

Kraus, H. J., J. Malcher, and E. Schaller (1985), Nocturnal low-level jet during PUKK, *Boundary Layer Meteorol.*, *38*, 1–22.

Laurent, B., B. Marticorena, G. Bergametti, J. F. Léon, and N. M. Mahowald (2008), Modeling mineral dust emissions from the Sahara desert using new surface properties and soil database, *J. Geophys. Res.*, *113*, D14218, doi:10.1029/2007JD009484.

Lenschow, D. H., and B. Stankov (1979), The rapid morning boundary-layer transition, *J. Atmos. Sci.*, *36*, 2108–2124.

Mahowald, N., R. G. Bryant, J. del Corral, and L. Steinberger (2003), Ephemeral lakes and desert dust sources, *Geophys. Res. Lett.*, *30*(2), 1074, doi:10.1029/2002GL016041.

Mahowald, N. M., A. R. Baker, G. Bergametti, N. Brooks, R. A. Duce, T. D. Jickells, N. Kubilay, J. M. Prospero, and I. Tegen (2005), Atmospheric global dust cycle and iron inputs to the ocean, *Global Biogeochem. Cycles*, *19*, GB4025, doi:10.1029/2004GB002402.

Mahrt, L. (1999), Stratified atmospheric boundary layers, *Boundary Layer Meteorol.*, *90*, 375–396.

Marticorena, B., and G Bergametti (1995), Modeling the atmospheric dust cycle: 1. Design of a soil-derived dust emission scheme, *J. Geophys. Res.*, *100*(D8), 16,415–16,430.

Mauritsen, T., and G. Svensson (2007), Observations of stably stratified shear-driven atmospheric turbulence at low and high Richardson numbers, *J. Atmos. Sci.*, *64*(2), 645–655, doi:10.1175/JAS3856.1.

May, P. T. (1995), The Australian nocturnal jet and diurnal variations of boundary-layer winds over Mt. Isa in north-eastern Australia, *Q. J. R. Meteorol. Soc.*, *121*, 987–1003.

Middleton, N. J., and A. S. Goudiev (2001), Saharan dust: Sources and trajectories, *Trans. Inst. Br. Geogr.*, *26*, 165–181.

Miller, R., and I. Tegen (1999), Radiative forcing of a tropical direct circulation by soil dust aerosols, *J. Atmos. Sci.*, *56*, 2403–3433.

Milton, S. F., G. Greed, M. E. Brooks, J. Haywood, B. Johnson, R. P. Allan, A. Slingo, and W. M. F. Grey (2008), Modeled and observed atmospheric radiation balance during the West African dry season: Role of mineral dust, biomass burning aerosol, and surface albedo, *J. Geophys. Res.*, *113*, D00C02, doi:10.1029/2007JD009741.

Nappo, C. J. (1991), Sporadic breakdowns of stability in the PBL over simple and complex terrain, *Boundary Layer Meteorol.*, *54*, 69–87.

Nicholson, S. E. (2000), The nature of rainfall variability over Africa on times scales of decades to millenia, *Global Planet. Change*, *26*, 137–158.

Parker, D. J., R. R. Burton, A. Diongue-Niang, R. J. Ellis, M. Felton, C. M. Taylor, C. D. Thorncroft, P. Bessemoulin, and A. M. Tompkins (2005), The diurnal cycle of the West African monsoon circulation, *Q. J. R. Meteorol. Soc.*, *131*, 2839–2860, doi:10.1256/qj.04.52.

Pedgley, D. E. (1972), Desert depresssion over north-east Africa, *Meteorol. Mag.*, *101*, 228–244.

Peters, M., and G. Tetzlaff (1988), The structure of West African squall lines and their environmental moisture budget, *Meteorol. Atmos. Phys.*, *39*, 74–84.

Prezerakos, N. G., S. C. Michaelides, and A. S. Vlassi (1990), Atmospheric synoptic conditions associated with the initiation of north-west African depression, *Int. J. Climatol.*, *10*, 711–729.

Prospero, J. M., P. Ginoux, O. Torres, S. E. Nicholson, and T. E. Gill (2002), Environmental characterization of global sources of atmospheric soil dust identified with the Nimbus 7 Total Ozone Mapping Spectrometer (TOMS) absorbing aerosol product, *Rev. Geophys.*, *40*(1), 1002, doi:10.1029/2000RG000095.

Reiter, E. R., and R. F. Lester (1968), Richardson's number in the free atmosphere, *Arch. Meteorol. Geophys. Bioklimatol., Ser. A*, *17*, 1–7.

Schepanski, K., I. Tegen, B. Laurent, B. Heinold, and A. Macke (2007), A new Saharan dust source activation frequency map derived from MSG-SEVIRI IR-channels, *Geophys. Res. Lett.*, *34*, L18803, doi:10.1029/2007GL030168.

Schmetz, J., P. Pili, S. Tjemkes, D. Just, J. Kerkmann, S. Rota, and A. Ratier (2002), An introduction to Meteosat Second Generation (MSG), *Bull. Am. Meteorol. Soc.*, *83*, 977–992.

Smith, R. K., and M. J. Reeder (1988), On the movement and low-level structure of cold fronts, *Mon. Weather Rev.*, *116*, 1927–1943.

Sokolik, I. N., and O. B. Toon (1996), Direct radiative forcing by anthropogenic mineral aerosols, *Nature*, *381*, 681–683.
Sorbjan, Z. (2006), Local structure of turbulence in stably stratified boundary layers, *J. Atmos. Sci.*, *63*, 1526–1537.
Steppler, J., G. Doms, U. Schättler, H. W. Bitzer, A. Gassmann, U. Damrath, and G. Gregoric (2003), Meso-gamma scale forecast using the nonhydrostatic model LM, *Meteorol. Atmos. Phys.*, *82*, 75–96.
Sutton, L. J. (1925), Haboobs, *Q. J. R. Meteorol. Soc.*, *51*(213), 25–30.
Tegen, I., and A. A. Lacis (1996), Modeling of particle size distribution and its influence on the radiative properties of mineral dust aerosol, *J. Geophys. Res.*, *101*(D14), 19,237–19,244.
Tegen, I., S. P. Harrison, K. Kohfeld, and I. C. Prentice (2002), Impact of vegetation and preferential source areas on global dust aerosol: Results from a model study, *J. Geophys. Res.*, *107*(D21), 4576, doi:10.1029/2001JD000963.
Thorncroft, C. D., and H. A. Flocas (1997), A case study of Saharan cyclogenesis, *Mon. Weather Rev.*, *125*, 1147–1165.
Thorpe, A. J., and T. H. Guymer (1977), The nocturnal jet, *Q. J. R. Meteorol. Soc.*, *103*, 633–653.
Tiedtke, M. (1989), A comprehensive mass flux scheme for cumulus parameterisation in large-scale models, *Mon. Weather Rev.*, *117*, 1779–1799.
Todd, M. C., R. Washington, S. Raghavan, G. Lizcano, and P. Knippertz (2008), Regional model simulations of the Bodélé low-level jet of northern Chad dudring the Bodélé Dust Experiment (BoDEx 2005), *J. Clim.*, *21*, 995–1012, doi:10.1175/2007JCLI1766.1.
Torres, O., A. Tanskanen, B. Veihelmann, C. Ahn, R. Braak, P. K. Bhartia, P. Veefkind, and P. Levelt (2007), Aerosols and surface UV products from Ozone Monitoring Instrument observations: An overview, *J. Geophys. Res.*, *112*, D24S47, doi:10.1029/2007JD008809.
Trigo, I. F., G. R. Bigg, and T. D. Davies (2002), Climatology of cyclogenesis mechanisms in the Mediterranean, *Mon. Weather Rev.*, *130*, 549–569.
Tulet, P., M. Mallet, V. Pont, J. Pelon, and A. Boone (2008), The 7–13 March 2006 dust strom over West Africa: Generation, transport, and vertical stratification, *J. Geophys. Res.*, *113*, D00C08, doi:10.1029/2008JD009871.
Uppala, S., et al. (2005), The ERA-40 re-analysis, *Q. J. R. Meteorol. Soc.*, *131*, 2961–3012.
Washington, R., and M. C. Todd (2005), Atmospheric controls on mineral dust emission from the Bodélé Depression, Chad: The role of the low level jet, *Geophys. Res. Lett.*, *32*, L17701, doi:10.1029/2005GL023597.
Washington, R., M. Todd, N. J. Middleton, and A. S. Goudie (2003), Dust-storm source areas determined by the Total Ozone Monitoring Spectrometer and surface observations, *Ann. Assoc. Am. Geogr.*, *93*(2), 297–313.
Washington, R., et al. (2006), Links between topography, wind, deflation, lakes and dust: The case of the Bodele depression, Chad, *Geophys. Res. Lett.*, *33*, L09401, doi:10.1029/2006GL025827.
Westphal, D. L., O. B. Toon, and T. N. Calson (1988), A case study of mobilization and transport of Saharan dust, *J. Atmos. Sci.*, *45*(15), 2145–2175.
Wolke, R., O. Knoth, O. Hellmuth, W. Schröder, and E. Renner (2004a), The parallel model system LM-MUSCAT for chemistry-transport simulations: Coupling scheme, parallelization and application, in *Parallel Computing: Software Technology, Algorithms, Architectures and Applications*, *Adv. in Parallel Comput.*, vol. 13, edited by G. R. Joubert et al., pp. 363–370, Elsevier, Amsterdam, Netherlands.
Wolke, R., O. Hellmuth, O. Knoth, W. Schröder, B. Heinrich, and E. Renner (2004b), The chemistry-transport modeling system LM-MUSCAT: Description and CityDelta applications, in *Air Pollution Modeling and Its Application XVI*, edited by C. Borrego and S. Incecik, pp. 427–437, Kluwer Acad., New York.
Yang, G.-Y., and J. Slingo (2001), The diurnal cycle of the tropics, *Mon. Weather Rev.*, *129*, 784–801.
Zender, C. S., and D. Newman (2003), Spatial heterogeneity in aeolian erodibility: Uniform, topographic, geomorphic, and hydrologic hypotheses, *J. Geophys. Res.*, *108*(D17), 4543, doi:10.1029/2002JD003039.

G. Bönisch, Max-Planck-Institute for Biogeochemistry, D-07745 Jena, Germany.
B. Heinold, B. Laurent, K. Schepanski, and I. Tegen, Leibniz Institute for Tropospheric Research, Permoser Straße 15, D-04318 Leipzig, Germany. (kerstin.schepanski@tropos.de)
A. Macke, Leibniz Institute of Marine Sciences at University of Kiel (IFM-GEOMAR), West Shore Campus, Düsternbrooker Weg 20, D-24105 Kiel, Germany.
M. C. Todd, Department of Geography, University College London, London WC1E 6BT, UK.